Accepted Manuscript

Evaluation of anticancer effect in vitro and in vivo of iridium(III) complexes on gastric carcinoma SGC-7901□cells

Wen-Yao Zhang, Yang-Jie Wang, Fan Du, Miao He, Yi-Ying Gu, Lan Bai, Lin-Lin Yang, Yun-Jun Liu

PII: S0223-5234(19)30520-3

DOI: https://doi.org/10.1016/j.ejmech.2019.06.003

Reference: EJMECH 11406

To appear in: *European Journal of Medicinal Chemistry*

Received Date: 18 April 2019

Revised Date: 23 May 2019

Accepted Date: 2 June 2019

Please cite this article as: W.-Y. Zhang, Y.-J. Wang, F. Du, M. He, Y.-Y. Gu, L. Bai, L.-L. Yang, Y.-J. Liu, Evaluation of anticancer effect in vitro and in vivo of iridium(III) complexes on gastric carcinoma SGC-7901□cells, *European Journal of Medicinal Chemistry* (2019), doi: https://doi.org/10.1016/j.ejmech.2019.06.003.

Graphical abstract

Three new iridium(III) complexes were synthesized and characterized. The cytotoxicity in vitro and in vivo was investigated. The complexes show high anticancer activity in vitro and in vivo.

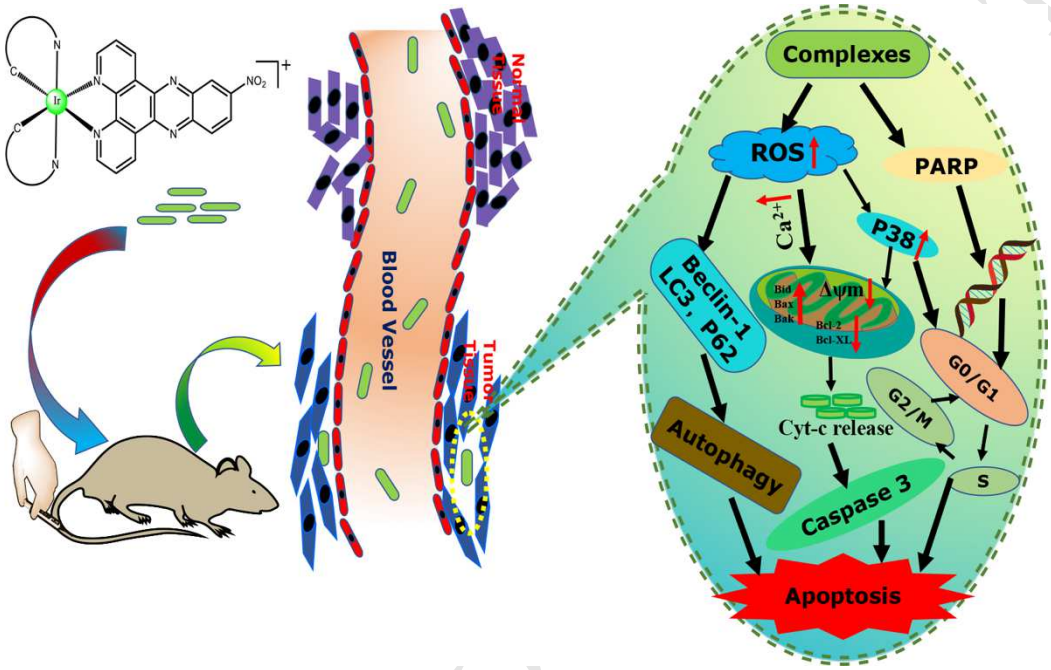

Submitted to Eur J Med Chem.

Evaluation of anticancer effect in vitro and in vivo of iridium(III) complexes on gastric carcinoma SGC-7901 cells

Wen-Yao Zhang[a], Yang-Jie Wang[a], Fan Du[a], Miao He[a], Yi-Ying Gu[a], Lan Bai[a], Lin-Lin Yang[b,*], Yun-Jun Liu[a,c*]

[a]*School of Pharmacy, Guangdong Pharmaceutical University, Guangzhou, 510006, P.R. China*

[b]*Department of Pediatrics, Guangdong Women and Children Hospital, Guangzhou 510000, P.R. China*

[c]School of Chemistry and Chemical Engineering, Guangdong Pharmaceutical University, Zhongshan, 528458, P.R. China.

*Corresponding author. *E-mail address:* fy_yanglinlin@126.com (L.L. Yang);

lyjche@gdpu.edu.cn (Y. J. Liu).

Abstract This work mainly introduces the synthesis and characterization of three iridium(III) complexes $[Ir(ppy)_2(adppz)](PF_6)$ (**Ir-1**), $[Ir(bzq)_2(addpz)](PF_6)$ (**Ir-2**) and $[Ir(piq)_2(adppz)](PF_6)$ (**Ir-3**). The complexes are more cytotoxic than cisplatin against tumor cell lines such as SGC-7901, A549, HeLa, Eca-109, HepG2 and BEL-7402. The toxicity test results indicated that complexes **Ir-1**, **Ir-2** and **Ir-3** can effectively inhibit the cell growth of SGC-7901 cells, and the measured IC_{50} values are 1.8 ± 0.4, 1.6 ± 0.3 and 0.8 ± 0.1 μM, respectively. AO/EB staining and flow apoptosis confirmed that SGC-7901 cells were caused apoptosis after being treated with the complexes. Along with the increase of endogenous ROS and Ca^{2+} levels, mitochondrial membrane potential collapse and massive release of cytochrome c, it is fully demonstrated that these complexes induce apoptosis through ROS-mediated mitochondrial pathway. At the same time, the complex **Ir-3** is outstanding in the inhibition of tumor growth in vivo. Combined with the above results, it provides a favorable foundation for the future development of more effective anti-tumor drugs.

Keywords: Iridium(III) complexes; Cytotoxicity in vitro and vivo; Apoptosis; Cell cycle arrest; western blot.

1. Introduction

Cancer is the most deadly disease in the world today, with liver, stomach, lung,

ovary and rectal cancer being the most common cancers with high mortality [1-3]. The easy transfer of tumor cells and rapid and excessive proliferation are the main challenges of cancer treatment [4-7]. Therefore, the design and development of effective anti-tumor drugs with outstanding tumor cytotoxicity and apoptotic rate and better inhibition of tumor spread have attracted much attention in the field of drug research and development. At present, metal platinum drugs (cisplatin, carboplatin, oxaliplatin) can effectively treat various types of cancer and have been successfully applied clinically [8-13]. However, with the continuous use in the clinic, the serious toxic and side effects of platinum drugs, drug resistance and selectivity are quickly exposed to the public's field of vision [14-18]. This drawback has quickly stimulated the exploration of other metal drugs by various scientific research groups around the world, and strived to find drugs that can reduce side effects, expand the spectrum of sensitive tumors, and try to overcome resistance. Among many metal drugs, organometallic iridium(III) complexes have been paid great attention by virtue of their rich functionality, multiple oxygen states and excellent photosensitivity [18-23]. Some iridium(III) complexes reveal high anticancer and antibacterial activity and can effectively inhibit the cancer cell proliferation [24-40]. To obtain more information on anticancer activity of iridium(III) complexes, in this paper, a ligand 11-nitrodipyrido[3,2-*a*:2',3'-*c*]phenazine (NDPPZ) and its three iridium(III) complexes: $[Ir(ppy)_2(NDPPZ)](PF_6)$ (ppy = 2-phenylpyridine, **Ir-1**), $[Ir(bzq)_2(NDPPZ)](PF_6)$ (bzq = benzo[h]quinolone, **Ir-2**) and $[Ir(piq)_2(NDPPZ)](PF_6)$ (piq = 1-phenylisoquinoline, **Ir-3**, Scheme 1) were synthesized and characterized by

elemental analysis, ESI-MS, ^{1}H NMR and ^{13}C NMR. The cytotoxicity of the complexes against cancer SGC-7901, A549, HepG2, BEL-7402, Eca-109 and normal NIH3T3 cells was evaluated by 3-(4,5-dimethylthiazole)-2,5-diphenyltetraazolium bromide (MTT) methods. The cellular morphological apoptosis, cell substructure localization, Ca^{2+} level, cytochrome c content and cytoskeleton were detected and analyzed by high-content cell imaging system. Apoptosis rate, cell cycle arrest, ROS level and mitochondrial membrane potential into the SGC-7901 cells were detected. In addition, we have conducted research on tumor invasion assay and molecular protein expression in order to further understand the apoptotic mechanism. The results of nude mice experiments further illustrate the inhibitory effect of iridium complexes on tumor cell growth, and effectively support the possibility that iridium complexes will become clinical anti-tumor drugs in the future. Finally, we hope this work can contribute to the development of anti-cancer drugs.

2. Results and discussion

2.1. In vitro growth inhibitory activity

The anticancer activities of complexes (**Ir-1**-**Ir-3**) were evaluated against six tumor cell lines: SGC-7901 (human gastric cancer cell line), A549 (human pulmonary adenocarcinoma cell), HeLa (human cervical carcinoma cell line), Eca-109 (human esophageal cancer cell line), HepG2 (Human hepatocellular liver carcinoma cell line), BEL-7402 (Human hepatocellular liver carcinoma cell line)) and normal cell NIH3T3

(3T3-Swiss albino) using MTT methods [41-43]. Cisplatin was used as a positive control. The IC_{50} values of the complexes toward the above cell lines are listed in Table 1. As an expectation, ligand NDPPZ shows low or no cytotoxicity toward the selected cancer cells. From table 1, all the complexes show strong toxicity against the cancer cell lines, especially SGC-7901 cells with a low IC_{50} value of 1.8 ± 0.4 μM for **Ir-1**, 1.6 ± 0.3 μM for **Ir-2** and 0.8 ± 0.1 μM for **Ir-3**. In addition, the results also indicate that antitumor activity of the complexes follows the order of **Ir-3** > **Ir-2** > **Ir-1** toward SGC-7901 cells. Complex **3** reveals the highest cytotoxicity in vitro among the three complexes against SGC-7901 and A549 cells. According to our previous work [41], we infer that this may be caused by large hydrophobicity of piq compared with ppy or bzq, which makes it easy for complex **3** to enter into the cells. On the other hand, $-NO_2$ as substituent group may increase the hydrophobicity of the complexes. Hence, these complexes exhibit high anticancer activity toward the selected cancer cells. However, for A549 cells, the anticancer activity of the complexes follows the order of **Ir-3** > **Ir-1** > **Ir-2**. Hence, we conclude that different complexes show different anticancer effect on the different cancer cells. In addition, the complexes reveal higher cytotoxic activity than cisplatin against the selected cancer cells under identical conditions. Because the complexes are sensitive to SGC-7901 cell, therefore, this cell line was selected for undergoing the following experiments. In order to observe whether the luminescence spectra of the complexes perturb the green fluorescence in the all cell experiments, the luminescence spectra of complexes **Ir-1**, **Ir-2** and **Ir-3** were determined in PBS solution at ambient

temperature. As shown in Fig. S1 (supporting information), **Ir-1**, **Ir-2** and **Ir-3** can emit at 599 nm, 595 nm and 605 nm, respectively. Whereas the emission wavelengths of DCHF-DA for ROS, JC-1 for mitochondrial membrane potential, Fluo-3AM for intracellular Ca^{2+} concentration and cyto c are 525 nm, 529 525 nm and 454 nm, respectively. Hence, the emission data of the complexes do not perturb the cell experiments.

2.2. Location and change of mitochondrial membrane potential (MMP)

The MTT data indicated that the Ir(III) complexes **Ir-1**, **Ir-2** and **Ir-3** have significant antiproliferative activity. As one of the most important subcellular structures, mitochondria participate in cellular energy production and apoptotic signaling pathways [44]. To affirm whether the mitochondria are a target, we used tracer dye Mito Tracker ® Deep Red FM (Thermo Fisher, 100 nM) [45] to further explore whether the complexes locate at the mitochondria. As shown in Fig. 1A, the mitochondria were stained red by Mito Tracker Red FM, complexes **Ir-1**, **Ir-2** and **Ir-3** emitted green fluorescence when SGC-7901 cells were treated with 2.0 μM of **Ir-1**, **Ir-2** and 1.0 μM of **Ir-3** for 6 h. It is worth noting when we overlay the red and green images, we will surprisingly find that the two images can be completely integrated. In other words, these complexes have a certain degree of targeting to mitochondria.

It is well known that the earliest change in apoptosis is the decrease in

mitochondrial membrane potential. To investigate whether these metal complexes induce apoptosis in mitochondria-mediated manner, We measured the change of mitochondrial membrane by loading SGC-7901 cells with fluorescent probe JC-1 (5,5',6,6'-tetrachloro-1,1',3,3'-tetraethylbenzimidazolocarbocyanine iodide) [46,47]. It is convenient to detect the change of mitochondrial membrane potential according to the change of fluorescent color. When the mitochondrial membrane potential is at a high potential, JC-I can accumulate in the mitochondrial matrix and emit red fluorescence. Conversely, if it is not able to accumulate in the mitochondrial matrix, the JC-1 monomer will emit green fluorescence. As depicted in Fig. 1B, It is clear that the red fluorescence was gradually replaced by green fluorescence on addition of Ir(III) complexes into SGC-7901 cells. Therefore, the experimental results indicate that complexes **Ir-1**-**Ir-3** can cause destruction of mitochondrial membrane integrity and decrease in transmembrane potential in SGC-7901 cells. Thus the results confirmed that mitochondria are involved in mediating apoptosis.

To investigate whether there is a correlation between mitochondrial membrane potential and reactive oxygen species, the changes in the mitochondrial membrane potential caused by the complexes in the presence of NAC [48] were further quantified. The relative ratio of red/green fluorescence intensity after the complexes treated SGC-7901 cells was determined by flow cytometry, which in turn reflected the mitochondrial depolarization ratio. As shown in Fig. 1C, in the control (a) or in the presence of NAC (b), the ratios of red/green are 11.97 and 19.41, respectively. Treatment of SGC-7901 cells with 1.0 μM of **Ir-1** (c), 2.0 μM of **Ir-1** (d) and **Ir-1** (2.0

μM) + NAC (8 μM) (e), 1.0 μM of **Ir-2** (f), 2.0 μM of **Ir-2** (g) and **Ir-2** (2.0 μM) + NAC (8 μM) (h), 0.5 μM of **Ir-3** (i), 1.0 μM of **Ir-3** (g) and **Ir-3** (1.0 μM) + NAC (8 μM) (k) for 24 h, the ratios of the red/green fluorescence are 1.24, 0.095 and 0.81 for **Ir-1**, 0.91, 0.16 and 0.33 for **Ir-2**, 2.98, 0.38 and 1.68 for **Ir-3**, respectively. According to the above experimental data, we can summarize two conclusions: (I) the complexes (**Ir-1**, **Ir-2** and **Ir-3**) exhibited dose tolerance to induce mitochondrial membrane potential collapse. (II) we can clearly see that in the presence of NAC, the red/green fluorescence ratio increases significantly compared with the complexes alone. The results indicate that NAC has an inhibitory effect on the collapse of mitochondrial membrane potential. Therefore, the accumulation of active oxygen will accelerate the decrease of mitochondrial membrane potential.

2.3. Intracellular ROS measurements

Endogenous reactive oxygen species (ROS) are considered to be key factors in cell signaling pathways, especially in terms of apoptosis and inflammation [49-51]. Regulating the homeostasis of reactive oxygen species in the body has become an important research direction for antitumor. In order to gain a deep understanding of the anti-tumor mechanism of these complexes, we used the specific fluorescent probe DCFH-DA to detect changes in the reactive oxygen species in SGC-7901 cells. As shown in Fig. 2A, in the control (a), a weakly green fluorescence points could be observed. However, SGC-7901 cells were incubated with Rosup (b, positive control), 2.0 μM of **Ir-1** (c), 2.0 μM of **Ir-2** (d) and 1.0 μM of **Ir-3** (e) for 24 h, a number of

green fluorescence points were found notably. Moreover, we further quantified the fluorescence intensity of the treated cells by flow cytometry. As see from Fig. 2B, SGC-7901 cells were exposed to **Ir-1**-**Ir-3** for 24 h in the absence or presence of NAC, the DCF fluorescent intensity increases 28.86, 16.81 and 19.55 times than that in the control, and the effect of **Ir-1**-**Ir-3** on the ROS levels were higher than Rosup group. The data obtained from Fig.2A and 2B suggest that these complexes can significantly increase the level of cellular reactive oxygen species, and that the complex **Ir-1** induces the production of reactive oxygen species more strongly than other complexes. The results demonstrate that NAC inhibits the production of cellular ROS.

Superoxide anion is one of the important components of intracellular ROS, which can cause damage to DNA and RNA at high concentrations. The determination of intracellular superoxide anion content was performed using fluorescent probe dihydroethidium (DHE) [52]. The probe DHE will be dehydrogenated by the intracellular superoxide anion to form the ethidium. Ethidium produces clear, bright red fluorescence when combined with DNA or RNA. As shown in Fig. 2C, in the control (a), weak red fluorescence could be observed. However, SGC-7901 cells were incubated with 2.0 μM of **Ir-1** (b), 2.0 μM of **Ir-2** (c) and 1.0 μM of **Ir-3** (d) for 24 h, a plentiful of red fluorescence points were observed clearly. To quantitatively compare the effects of complexes on $O_2^{\cdot -}$ levels, the DHE fluorescent intensity was determined by ImageXpress Micro XLS system (MD company, US) in the presence or absence of NAC. As shown in Fig. 2D, SGC-7901 cells were exposed to **Ir-1**-**Ir-3** for 24 h, the DHE fluorescent intensity increases 70.80, 62.17 and 89.09 times than

that in the control. The obtained results indicate that complexes can significantly increase the level of $O_2^{\bullet-}$ in SGC-7901 cells, while NAC can inhibit the production of $O_2^{\bullet-}$ in cells.

As a reactive oxygen molecule, NO plays an important role in the anti-tumor process. The endogenous NO level of cells can be conveniently detected using the fluorescent probe 3-amino-4-aminomethyl-2',7'-difluorescein diacetate (DAF-FMDA). As indicated in Fig. 2E, treatment of SGC-7901 cells displays an obvious green fluorescence after incubation with complexes (**Ir-1**-**Ir-3**) in comparison with the untreated cells. Then, we also quantitatively evaluate the endogenous NO levels. As shown in Fig. 2F, SGC-7901 cells were exposed to **Ir-1**-**Ir-3** for 24 h, the DAF-FMDA fluorescent intensity increases 1.09, 1.81 and 2.24 times than the control. Combined with the data above, complexes can increase the intracellular ROS levels.

As a major member of the MAPK pathway, P38 MAPK plays an important role in the regulation of various physiological signals such as cell stress, inflammation, apoptosis and cell cycle [53-57]. High levels of the intracellular ROS can activate the downstream protein P38 to induce apoptosis. Activation of P38 protein is essential for inducing cell apoptosis. Therefore, we assayed the expression of P38 protein after the treatment of SGC-7901 cells with complexes **Ir-1**-**Ir-3** by western blotting. See from Fig. 2G, we can clearly observe that the protein expression of P38 is significantly up-regulated after 24 h of exposure of SGC-7901 cells to the complexes. Therefore, these results showed that the complexes can increase the intracellular ROS level, and then induced apoptosis of SGC-7901 cells through ROS-P38 signaling pathway.

2.4. Apoptosis assay with AO/EB and Annex V/PI double staining methods

The MTT results indicated that the complexes have a significant effect on reducing the proliferation of SGC-7901 cells. To further understand the effect on apoptosis, the AO/EB and Annex V/PI double staining methods [58-60] were carried out to assess the changes in nuclear morphology and the degree of apoptosis. SGC-7901 cells stained with acridine orange (AO) and ethidium bromide (EB) are shown in Fig. 3A. In the control (a), the living cells were stained bright green and exhibited homogeneous nuclei staining in spots. After the treatment of SGC-7901 cells with 1.0 μM of **Ir-1** (b), 1.0 μM **Ir-2** (c), and 0.5 μM **Ir-3** (d) for 24 h, the apoptotic morphological features such as cell blebbing, nuclear shrinkage, chromatin condensation and fragmentation, as well as red necrotic cells, were observed. In order to more accurately quantify the effect of apoptosis, flow cytometry was used to study the proportion of apoptosis in cells treated with the complexes. As show in Fig. 3B, quantitative results showed that the early apoptosis rate of cells in SGC-7901 cells (a) treated with **Ir-1** (b, 1.0 μM), **Ir-2** (c, 1.0 μM) and **Ir-3** (d, 0.5 μM) for 48 h was 8.36%, 13.50% and 11.20%, respectively. The results indicate that the complexes can induce early apoptosis in SGC-7901 cells.

2.5. DNA damage assay

Elevated levels of intracellular ROS mediate DNA oxidative damage and ultimately induce apoptosis [61-63]. Comet assay as a most commonly used means to

assess genotoxicity was implemented in current study to evaluate the complexes inducing DNA damage. As shown in Fig. 4, it is clearly to see no DNA damage in the control (a). However, after SGC-7901 cells were incubated with 1.0 μM of **Ir-1** (b), 1.0 μM of **Ir-2** (c) and 0.5 μM of **Ir-3** (d) for 24 h, obviously and clearly-formed comets were observed. The results demonstrate that the complexes can induce DNA damage which further triggers apoptosis.

2.6. Autophagy induced by the complexes

Recent studies have shown that there is a close relationship between autophagy and the occurrence of tumor cells, especially when the cells are autophagic, which can cause tumor cell apoptosis [64]. To further explore the mechanism of apoptosis induced by the complex, the assessment of intracellular autophagy in SGC-7901 was detected by the specific dye monodansylcadaverine (MDC), and the intensity of fluorescence reflected the degree of autophagy [65]. The autophagy image is shown in Fig. 5A, we could find the weak fluorescence in the control (a). After the treatment of SGC-7901 cells with **Ir-1**-**Ir-3** for 24 h, bright green fluorescent cycles were observed, which suggests that complexes **Ir-1**-**Ir-3** can induce autophagy with the formation of autophagic vacuoles. The process of autophagy is always accompanied by some key protein expression such as LC3, Beclin-1 and p62. The proteins LC3-II and Beclin-1 are directly involved in the formation of autophagosomes, and the content of LC3-II is directly proportional to the content of autophagic vesicles [66]. As a substrate for autophagosome formation, the level of protein p62 will decrease when a large amount

of autophagy occurs. Therefore, Western blotting was used to assess the expression of individual proteins in SGC-7901 cells. As depicted in Fig. 5B, after SGC-7901 cells were treated with the complexes, the expression level of p62 protein was significantly down-regulated, whereas the expression levels of Beclin-1 and LC3-II showed an increasing trend, and the LC3-II/LC3-I ratio increased significantly. The results of the data indicate that the complexes can induce autophagy.

It is well known that the relationship between autophagy and the proliferation of tumor cells is twofold. On one hand, autophagy can prompt cell proliferation; On the other hand, autophagy can inhibit the cell proliferation. To understand the relationship between autophagy and cell proliferation, the viability of SGC-7901 cells was assessed by the MTT method in the presence of 3-MA or NAC. As shown in Fig. 6, in the presence of NAC (**Ir-1**-**Ir-3** + NAC, yellow line) and 3-MA (**Ir-1**-**Ir-3** + 3MA, purple line), NAC induce an increase of the cell viability compared with **Ir-1**-**Ir-3** (blue line), but 3-MA induces more cell death. All of the above data indicate that autophagy prompts cell proliferation, whereas high levels of reactive oxygen species (ROS) accelerate cell death.

2.7. Determination of intracellular Ca^{2+} levels

It is currently accepted that the transduction of intracellular related signals and the implementation of the pre-apoptotic phase are inseparable from the involvement of Ca^{2+} [67]. High levels of reactive oxygen species (ROS) will open the mitochondrial permeability transition pores and will increase calcium uptake in the mitochondria.

Once Ca^{2+} overload occurs in the mitochondria, cytochrome c is released to activate caspase, and finally apoptosis will occur [68]. Therefore, we evaluate changes in intracellular Ca^{2+} levels after the treatment of SGC-7901 cells with the complexes using the specific fluorescent probe Fluo-3AM. As shown in Fig. 7A, the green fluorescence of the experimental group (c for **Ir-1**, d for **Ir-2** and e for **Ir-3**) was significantly stronger than that of the control group (a). However, in the absence of Ca^{2+} free medium (b), the green fluorescence is similar to the control. Next, we further quantified the fluorescence intensity. It is apparent from Fig. 7B that the fluorescence intensity of the control group is lower than that of the complexes-treated groups, whereas in the absence Ca^{2+} free medium, the fluorescence intensity is slight high compared with the control. The data confirmed that the complexes can significantly increase the intracellular Ca^{2+} level.

2.8. Release of cytochrome c

As the main electron carrier in the mitochondrial respiratory chain, cytochrome c is a key factor in cell signal transduction [69]. Cytochrome c, a key factor in the process of apoptosis, is released into the cytoplasm and can bind to apoptosis-related factors and activate caspase-9, thereby triggering apoptosis [70]. It can be seen from Fig. 8A that the green fluorescence after the treatment of SGC-7901 cells with the complexes (**Ir-1**-**Ir-3**) was significantly stronger than that of the control group. The results indicate that cytochrome c can be released from mitochondria after the treatment of SGC-7901 cells with the complexes. In addition, the integrated

fluorescent intensity/cell was determined by Multi Wavelength Cell Scoring module. See from Fig. 8B, the green fluorescence increases by 4.37 times for **Ir-1**, 3.79 times for **Ir-2** and 4.58 times for **Ir-3** than that in the control. The experimental results demonstrate that the complexes can induce a release of cytochrome c.

2.9. Cell invasion assays

One of the main reasons for the lack of effective methods for cancer treatment is that tumor cells are easy to metastasize and spread [71]. Therefore, it is essential to evaluate the effects of the three complexes on inhibiting the metastatic spread of SGC-7901 cells. Invasion assay results are shown in Fig. 9A and B, and we can observe that these complexes have outstanding inhibitory effects on the invasion of SGC-7901 cells. Additionally, the percentage of inhibiting the cell invasion is 51.5% for **Ir-1**, 49.3% for **Ir-2** and 74.0% for **Ir-3** after SGC-7901 cells were exposed to 2.0 μM of the complexes, respectively. It is interesting to note that all complexes exhibit excellent concentration-dependent manner for cell invasion inhibition. All the above data results further reveal that the obtained complexes are effective on inhibiting cell migration.

2.10. Cell cycle analysis

The current research reveals that anticancer drugs show different degrees and properties for the tumor cell cycle [72,73]. Through the evaluation of the degree of cell cycle damage of SGC-7901 cells, a deep understanding of the mechanism of

apoptosis induced by complexes. To investigate the effects of the complexes on the cell cycle, flow cytometry analysis of SGC-7901 cells treated with dye iodized pyridine was used. As shown in Fig.10, flow cytometry results showed that deal with complexes for 24 h caused distinguished accumulation of cells in G0/G1 phase. Compared with the control (43.95%, Fig. 10a), the percentage of SGC-7901 cells in G0/G1 phase increased by 50.87% for **Ir-1** (b), 48.71% for **Ir-2** (c) and 54.24% for **Ir-3** (d) after treated with complexes for 24 h. The data clearly display that these complexes cause the cell cycle to be arrested at the G0/G1 phase.

2.11. Tubulin polymerization assay

In large number of studies on the morphology of cytoskeleton, it is found that changes in cytoskeletal structure are essential for the morphological changes of apoptotic cells [74]. Microtubules are not only the key in maintaining the morphological structure of cells, but also essential for the transport of substances and the transduction of signals [75]. Therefore, we labeled microtubules and cytoskeleton by immunofluorescent methods to further explore the mechanism of inhibition of SGC-7901 cell growth by complexes. As shown in Fig. 11, there was no change in the morphology of the microtubules in the control cells (a), and a perfect fusiform shape was exhibited. However, after treatment with the complexes **Ir-1** (b), **Ir-2** (c) and **Ir-3** (d) for 10 h, the cell microtubule structure exhibited a circular shape. The results confirmed that the complexes inhibited the microtubule polymerization and caused a significant change in the cytoskeleton morphology, eventually leading to cell

morphology collapse.

2.12. Assays of Bcl-2 family proteins by western blot

To further clarify the apoptotic mechanism induced by the complexes, we examined the expression of related protein molecules by Western Blot assay [76,77]. The early key apoptotic factor caspase-3 mediates the entire apoptotic event of cells after being activated by substrate-cleaved PARP [78]. The P-p53 tumor-associated gene, a cell-mediated signal transduction pathway plays an important role in regulating cell activities. As we all known, Bcl-2 and Bcl-xl inhibits apoptosis, whereas Bax, Bid and Bak stimulate apoptosis. As shown in Fig. 12, the results demonstrated that treatment of SGC-7901 cells with **Ir-1**-**Ir-3** led to activate caspase 3 and cleavage of PARP, which further confirms that the complexes can induce apoptosis in SGC-7901 cells. The treatment of SGC-7901 cells induces a decrease in the expression of phosphorylation of p53 (P-p53) and the antiapoptotic proteins Bcl-2 and Bcl-xL. Besides, the expression levels of Bax, Bid and Bak were up-regulated. Although complex **3** exhibits the highest anticancer activity against SGC-7901 cells among the three complexes, owing to different proteins with different structures, therefore, different complexes cause different up-regulation or down-regulation toward Bak or Bcl-xL. These results indicate that the complexes induce apoptosis through regulating the expression of Bcl-2 family proteins.

2.13. In vivo antitumor effect

The results of a series of in vitro experiments confirmed that the complexes showed excellent inhibitory effects on the proliferation against the tested tumor cells. The LD_{50} value measured by the 10-day acute toxicity test for **Ir-3** is 8.4 mg/Kg. Next, we implanted SGC-7901 cells into nude mice and grew corresponding transplanted tumors to further evaluate the inhibitory effect of **Ir-3** in vivo. The corresponding tumor volume and weight were measured and recorded in the control group, cisplatin (positive group) and nude mice treated with 0.75 mg/kg and 1.50 mg/kg **Ir-3** per day. As can be clearly seen from the data of Fig. 13A-D, after 7 days of treatment with **Ir-3**, the tumor growth inhibition effect was significantly higher than that of the control group. The inhibiting percentages of tumor growth induced by cisplatin, 0.75 mg/kg and 1.50 mg/kg are 30.71%, 37.97% and 43.93%, respectively (Fig. 13D). Complex **Ir-3** displays obvious antitumor activity, and the tumor inhibition rate is higher than cisplatin under identical condition. The results indicate that complex **Ir-3** reveals a concentration-dependent manner to inhibit the tumor growth.

Through the pathological analysis of tumors and tissues in Fig. 14, the following results can be obtained: in the blank control group, the lungs of the nude mice were congested with ablation of the alveolar septum, emphysema and local alveolar plaque hemorrhage. In the positive group, there were also symptoms such as pulmonary congestion and emphysema, but there were also lace-like changes in the tracheal wall and scattered small metastases. The lungs of nude mice treated with the complexes showed extensive alveolar hemorrhage except for the same condition as the positive group. In addition, there was no significant difference between the hearts of nude

mice in each group, which showed local myocardial eosinophilic changes and edema fractures. Similarly, we also observed that the liver tissue of each group showed visible focal cancer metastasis, small piece of hepatocyte necrosis and small piece of hemorrhage. The glomeruli of the three groups of nude mice showed congestion, tubular edema and interstitial siltation. There was no difference in brain tissue of each group of nude mice showing mild congestion and edema. At the same time, it can be observed that the tumor capsule is intact in the blank group, the growth is vigorous, the division phase is clearly visible, and the large-scale necrosis in the tumor. The tumor performance of the positive group was basically the same as that of the blank control, but the range of tumor necrosis was significantly reduced. The results after treatment with the complexes were not significantly different from those of the positive groups. Therefore, complex **Ir-3** may become a potent anti-tumor drug candidate in the future.

3. Conclusions

In the current study, three new compounds $[Ir(ppy)_2(NDPPZ)](PF_6)$ (**Ir-1**), $[Ir(bzq)_2(NDPPZ)](PF_6)$ (**Ir-2**) and $[Ir(piq)_2(NDPPZ)](PF_6)$ (**Ir-3**) were synthesized, characterized and evaluated for biological activity. The experimental data showed that the three complexes have the most prominent inhibitory effect on SGC-7901 cell proliferation. In vitro studies have shown that complexes can enhance endogenous ROS and calcium levels, thereby mitigating mitochondrial mode potential and inducing apoptosis in SGC-7901 cells. These complexes are excellent in inhibiting the

migration of tumor cells and inhibiting their growth at the G0/G1 phase. At the same time, the DNA damage of the cells is further explained by the results of the comet assay and the molecular expression level of the cleavage PARP. In addition, the complexes can also activate caspase-3 by promoting the release of cytochrome c in mitochondria, thereby inducing the regulation of Bcl-2 family protein expression. Finally, the in vivo activity evaluation results showed that the complex **Ir-3** has a significant inhibitory effect on tumor growth. In summary, the results of the above data indicate that the complexes induce apoptosis in SGC-7901 cells through the following three pathways (Fig. 15): (I) The complexes can significantly increase the level of endogenous reactive oxygen species (ROS) in the cells, and the excessive accumulation of ROS induces the production of autophagy, resulting in apoptosis; (II) Excessive reactive oxygen species cause Ca^{2+} loading after opening of the mitochondrial membrane permeability transition pore. At the same time, mitochondrial function is further destroyed, causing a large release of cytochrome c, leading to apoptosis; (III) The complexes damage cellular DNA by altering the expression of PARP protein, and block cell division in G0/G1 phase, promoting apoptosis. Hence, this work will be beneficial to the future anti-tumor mechanism and design of new Ir(III) complexes.

4. Experimental

4.1 Materials and methods

2-phenylpyridine, benzo[h]quinoline, 1-phenylisoquinoline, 1,10-phenanthroline,

4-nitrobenzene-1,2-diamine were purchased from Sigma-Aldrich and used without further purification unless otherwise noted. Ultrapure MilliQ water was used in all experiments. FBS and RPMI 1640 were purchased from Gibco company. Fluorescent dye kits and related consumables are sourced from Beyotime Biotechnology. The cancer SGC-7901, A549, HeLa, Eca-109, HepG2, BEL-7402 and normal NIH3T3 cell line were purchased from the American Type Culture Collection. $IrCl_3{\cdot}3H_2O$ was purchased from the Kunming Institution of Precious Metals.

Microanalysis (C, H, and N) was carried out with a PerkinElmer 240Q elemental analyzer. Electrospray ionization mass spectra (ESI-MS) were recorded on a LCQ system (Finnigan MAT, USA) using acetonitrile as the mobile phase. The spray voltage, tube lens offset, capillary voltage and capillary temperature were set at 4.50 kV, 30.00 V, 23.00 V and 200 □, respectively, and the quoted m/z values are for the major peaks in the isotope distribution. ^{1}H NMR and ^{13}C NMR spectra were recorded on a Varian-500 spectrometer with DMSO-d6 as a solvent and tetramethylsilane (TMS) as an internal standard at 500 MHz at room temperature.

4.2. Synthesis of complexes

*4.2.1. Synthesis of complex $[Ir(ppy)_2(NDPPZ)]PF_6$ (**Ir-1**)*

A mixture of cis-$[Ir(ppy)_2Cl]_2$ (0.28 g, 0.25 mmol) [79] and NDPPZ [80] (0.164 g, 0.50 mmol) were dissolved in dichloromethane and methanol mixed solution (V_{CH2Cl2}: V_{CH3OH} = 2:1), then the mixture was refluxed under argon for 6 h to appear a clear red brown solution. And then the solution was cooled to room temperature, a

large amount of yellow precipitated product appeared after the dropwise addition of ammonium hexafluorophosphate and stirring for 2 h. The crude complex was purified by column chromatography on neutral alumina with dichloromethane-acetone (1:3, v/v) as eluent. After removing the solvent under reduced pressure and further drying, a bright yellow pure complex was obtained. Yield: 82%. Anal. Calc for $C_{40}H_{25}N_7O_2IrPF_6$: C, 49.38; H, 2.59; N, 10.08%. Found: C, 49.25; H, 2.69 N, 10.02%. ^{1}H NMR (DMSO-d_6, 500 MHz) (Fig. S2a, supporting information): δ 9.72 (dd, 2H, *J* = 5.5, *J* = 4.5 Hz), 9.23 (d, 1H, *J* = 2.5 Hz), 8.77 (d, 1H, *J* = 7.0 Hz), 8.69 (d, 1H, *J* = 9.5 Hz), 8.33 (d, 2H, *J* = 5.0 Hz), 8.28 (d, 2H, *J* = 8.0 Hz), 8.72-8.18 (m, 2H), 7.96 (d, 2H, *J* = 7.5 Hz), 7.91 (t, 2H, *J* = 8.0 Hz), 7.67 (t, 2H, *J* = 6.0 Hz), 7.09-7.04 (m, 4H), 6.97 (t, 2H, *J* = 7.5 Hz), 6.28 (d, 2H, *J* = 7.5 Hz). ^{13}C NMR (DMSO-d_6, 125 MHz) (Fig. S3a, supporting information): 166.85, 152.56, 152.41, 150.42, 150.14, 149.65, 149.51, 148.85, 144.08, 143.78, 142.66, 142.19, 140.58, 138.97, 135.69, 135.48, 131.56, 131.25, 130.47, 130.43, 128.94, 128.88, 125.57, 125.35, 125.22, 123.92, 122.68, 120.12. ESI-MS (CH_3CN): 828.0 ($[M - PF_6]^+$). HRMS (CH_3CN): 828.1678 ($[M - PF_6]^+$) (Fig. S4a, supporting information).

*4.2.2. Synthesis of complex [Ir(bzq)$_2$(NDPPZ)]PF$_6$ (**Ir-2**)*

Obtaining this complex by a method similar to that described for the synthesis of complex **Ir-1**, with $[Ir(bzq)_2Cl]_2 \cdot 2H_2O$ [79] in place of $[Ir(ppy)_2Cl]_2 \cdot 2H_2O$. Yield: 76%. Anal. Calc for $C_{44}H_{25}N_7O_2IrPF_6$: C, 51.77; H, 2.47; N, 9.60%. Found: C, 51.89; H, 2.35; N, 9.71%. ^{1}H NMR (DMSO-d_6, 500 MHz) (Fig. S2b, supporting

information): δ 9.70 (d, 2H, *J* = 8.0 Hz), 9.23 (d, 1H, *J* = 2.5 Hz), 8.78 (d, 1H, *J* = 6.5 Hz), 8.68 (d, 1H, *J* = 9.0 Hz), 8.53 (d, 2H, *J* = 8.0 Hz), 8.30 (t, 2H, *J* = 5.0 Hz), 8.14-8.07 (m, 4H), 7.98 (d, 2H, *J* = 9.0 Hz), 7.87 (d, 2H, *J* = 9.0 Hz), 7.58 (d, 2H, *J* = 8.0 Hz), 7.52-7.49 (m, 2H), 7.22 (t, 2H, *J* = 7.5 Hz), 6.31 (d, 2H, *J* = 7.0 Hz). ^{13}C NMR (DMSO-d_6, 125 MHz) (Fig. S3b, supporting information): 156.32, 153.09, 152.94, 150.85, 150.57, 149.38, 148.85, 146.29, 143.77, 142.67, 142.21, 140.57, 140.35, 137.81, 135.71, 135.48, 133.86, 131.55, 130.43, 130.38, 129.85, 129.59, 128.93, 128.87, 128.62, 126.81, 125.57, 125.35, 124.34, 122.81, 120.66. ESI-MS (CH_3CN): 876.0 ($[M - PF_6]^+$). HRMS (CH_3CN): 876.1687 ($[M - PF_6]^+$) (Fig. S4b, supporting information).

*4.2.3. Synthesis of complex [Ir(piq)$_2$(NDPPZ)]PF$_6$ (**Ir-3**)*

The complex is obtained by the same method as described in the synthesis of complex **Ir-1**, with $[Ir(piq)_2Cl]_2 \cdot 2H_2O$ [79] in place of $[Ir(ppy)_2Cl]_2 \cdot 2H_2O$. Yield: 78%. Anal. Calc for $C_{48}H_{29}N_7O_2IrPF_6$: C, 53.73; H, 2.72; N, 9.13%. Found: C, 53.82; H, 2.79; N, 9.01%. ^{1}H NMR (DMSO-d_6, 500 MHz) (Fig. S2c, supporting information): δ 9.73 (d, 2H, *J* = 6.5 Hz), 9.20 (d, 1H, *J* = 2.5 Hz), 9.02 (d, 2H, *J* = 8.5 Hz), 8.76 (d, 1H, *J* = 6.5 Hz), 8.67 (d, 1H, *J* = 9.5 Hz), 8.40 (d, 2H, *J* = 8.0 Hz), 8.20-8.15 (m, 4H), 8.05 (t, 2H, *J* = 6.5 Hz), 7.88 (t, 4H, *J* = 7.5 Hz), 7.56 (t, 2H, *J* = 6.5 Hz), 7.50 (dd, 2H, *J* = 6.0, *J* = 6.5 Hz), 7.18 (t, 2H, *J* = 7.5 Hz), 6.98 (t, 2H, *J* = 7.0 Hz), 6.28 (d, 2H, *J* = 7.5 Hz). ^{13}C NMR (DMSO-d_6, 125 MHz) (Fig. S3c, supporting information): 167.88, 152.87, 152.52, 152.36, 150.24, 149.95, 148.83, 145.43, 143.77, 142.65, 142.19,

141.21, 140.57, 136.67, 135.76, 135.54, 132.22, 131.68, 131.55, 130.79, 130.73, 130.55, 130.49, 129.51, 128.97, 128.92, 127.76, 126.53, 125.63, 125.54, 125.34, 122.65, 122.21. ESI-MS (CH_3CN): 928.07 ($[M - PF_6]^+$). HRMS (CH_3CN): 928.2034 ($[M - PF_6]^+$) (Fig. S4c, supporting information).

4.3. Cytotoxicity assay in vitro

Cancer cells suspension were seeded in 96-well microarray plates (1×10^4 cells per well) and incubated overnight at 37 °C in a 5% CO_2 incubator. All tested complexes were dissolved in DMSO, and the final concentration of the complexes ranged from 3.125-100 μM. The 96-well plates were incubated for 48 hours at 37 °C in a 5% CO_2 incubator. When the incubation is complete and the culture in the wells is removed, add 90 μL of the culture medium and 10 μL of the MTT dye solution (20 μL, 5 mg/mL) to each well. After 4 h, buffer (100 μL) containing dimethylformamide (50%) and sodium dodecyl sulfate (20%) was added to solubilize the MTT formazan. The microplate reader was used to measure the absorbance of each well at a wavelength of 490 nm. The IC_{50} values were determined by plotting the percentage of viable cells versus concentration on a logarithmic graph and reading off the concentration at which 50% of cells remain viable relative to the control. Each set of experiments must be repeated at least three times to calculate the average.

4.4. Localization assay of the complex in the mitochondria

SGC-7901 cells were placed in 12-well microassay culture plates (1×10^5 cells

per well) and grown overnight at 37 ^{o}C in a 5% CO_2 incubator. The compounds of the corresponding concentration were added to the wells at 37 ^{o}C in a 5% CO_2 incubator for 9 h and the cells were stained with MitoTracker Deep Red FM (150 nM) at 37 ^{o}C for 30 min. Upon completion of the incubation, the wells were washed three times with ice-cold PBS. After discarding the culture medium, the cells were imaged under ImageXpress Micro XLS system (MD company, US).

4.5. Mitochondrial membrane potential (MMP) assay

SGC-7901 cells in 12-well plates were treated with complexes **Ir-1**-**Ir-3** for 24 h, and then washed three times with 500 μL of cold PBS per well. The cancer cells are separated by using trypsin-EDTA solution. 1 μg/mL of JC-1 (5,5',6,6'-tetrachloro-1,1',3,3'-tetraethyl-imidacarbocyanine iodide) was used to dye the cells at room temperature for 20 minutes in the dark. The cells were immediately centrifuged to remove the supernatant. Then the cell pellets were suspended in PBS and imaged under ImageXpress Micro XLS system (MD company, US), and the ratio of red/green fluorescence intensity was determined by flow cytometry.

4.6. Reactive oxygen species (ROS) detection

4.6.1. Intracellular ROS levels detection

The specific fluorescent probe 2,7-dichloro-dihydrofluorescein diacetate (DCFH-DA) was used to investigate the changes of intracellular ROS levels. SGC-7901 cells were placed in a 12-well plate at a density of 1.5×10^5 per well. After

24 h, the medium in the wells was replaced with medium containing the corresponding concentration of **Ir-1**-**Ir-3** and incubation for 24 h. Finally, the cells pellets were suspended in PBS and imaged under ImageXpress Micro XLS system (MD company, US), and the DCF fluorescence intensity was calculated by flow cytometry.

4.6.2. Intracellular superoxide anion detection

The level of superoxide anion in cells is detected by DHE (Dihydroethidium) as a fluorescent probe. SGC-7901 cells were placed in a 12-well plate at a density of 1.5 × 10^5 per well. After 24 h, the medium in the wells was replaced with medium containing the corresponding concentration of **Ir-1**-**Ir-3** and incubation for 24 h. The cells were then treated in the dark for 30 min with PBS solution containing 10 μM DHE dye. Finally, the cells are imaged and the respective fluorescence intensities are calculated by using the ImageXpress Micro XLS system (MD company, US).

4.6.3. Intracellular nitric oxide level detection

DAF-FM DA (3-amino-4-aminomethyl-2',7'-difluorescein diacetate was used as fluorescence probe to determine the intracellular nitric oxide levels. SGC-7901 cells with a density of 1.5 × 10^5 per well were seeded in 12 wells and incubated overnight in an incubator. Next, replace the medium in the 12-well plate with the medium containing the corresponding concentration of **Ir-1**-**Ir-3** and continue to be incubated for 24 h. Finally, the cells are imaged and the respective fluorescence intensities are

calculated by using the ImageXpress Micro XLS system (MD company, US).

4.7. Apoptosis assay by AO/EB staining methods

Acridine orange and ethidium bromide (AO/EB) staining was used to detect the apoptotic morphology of SGC-7901 cells. SGC-7901 cells were placed in a 12-well plate at a density of 1.5×10^5 per well. After 24 h, the medium in the wells was replaced with medium containing the corresponding concentration of **Ir-1-Ir-3** and incubation for 24 h. Then the cells in the wells were washed with cold PBS, the cells were dyed by acridine range (AO) and ethidium bromide (EB) (AO: 100 μg/mL, EB: 100 μg/mL) for 10 min in the dark. The cells were imaged by ImageXpress Micro XLS system (MD company, US).

4.8. Apoptosis assay by flow cytometry

SGC-7901 cells in the 6-well plate were treated with **Ir-1-Ir-3** and collected by using a trypsin-EDTA solution. After the supernatant was removed and the cells were washed and stained with PBS solution containing 500 mg/mL pyridine iodide (PI) and 1 mg/mL annexin V-FITC for 20 min in a dark. The fluorescence was measured at 530 nm using 488 nm excitation with an FACS Calibur flow cytometer (Beckman Dickinson & Co., Franklin Lakes, NJ). A minimum of 10,000 cells were analyzed per sample.

4.9. DNA damage assay

DNA damage was investigated by means of comet assay. SGC-7901 cells in culture medium were incubated with complexes **Ir-1**, **Ir-2** and **Ir-3** at 37 °C for 24 h. The cells were harvested by a trypsinization process at 24 h. A total of 100 μL of 0.5% normal agarose in PBS was dropped gently onto a fully frosted microslide, covered immediately with a coverslip, and then placed at 4 °C for 10 min. The coverslip was removed after the gel has been fixed. 50 μL of the cell suspension (200 cells/μL) was mixed with 50 μL of 1% low melting agarose preserved at 37 °C. A total of 100 μL of this mixture was applied quickly on top of the gel, coated over the microslide, covered immediately with a coverslip, and then placed at 4 °C for 10 min. The coverslip was again removed after the gel has been fixed. A third coating of 50 μL of 0.5% low melting agarose was placed on the gel and allowed to place at 4 °C for 15 min. After solidification of the agarose, the coverslips were removed, and the slides were immersed in an ice-cold lysis solution (2.5 M NaCl, 100 mM EDTA, 10 mM Tris, 90 mM sodium sarcosinate, NaOH, pH 10, 1% Triton X-100 and 10% DMSO) and placed in a refrigerator at 4 °C for 2 h. All of the above operations were performed under low lighting conditions to avoid additional DNA damage. After the removal of the lysis solution, the slides were placed horizontally in an electrophoresis chamber. The reservoirs were filled with an electrophoresis buffer (300 mM NaOH, 1.2 mM EDTA) until the slides were just immersed in the buffer solution, and the DNA was allowed to unwind for 30 min in the electrophoresis solution. Then the electrophoresis was carried out at 25 V and 300 mA for 20 min. After electrophoresis, the slides were removed, and washed thrice in a neutralization buffer (400 mM Tris, HCl, pH 7.5).

Nuclear DNA was stained with 20 μL of EtBr (20 μg/mL) in the dark for 20 min. The slides were washed in chilled distilled water for 10 min to neutralize the excess alkali, air-dried and scored for comets by fluorescence microscopy. A total of 10 comets on each gel were scored.

4.10. Autophagy induced by the complexes

SGC-7901 cells were placed into a 12-well plate and incubate overnight. Replace the medium in the plate with a new medium containing the corresponding concentration of **Ir-1-Ir-3** and incubate for 24 h at 37 °C in a 5% CO_2 incubator. After the incubation was completed, the medium in the wells was removed and the cells were washed three times with cold PBS. The plated cells were then stained with MDC (monodansylcadaverine) solution (50 mM) for 20 minutes at 37 °C. Finally, the cells were imaged using the ImageXpress Micro XLS system (MD, US).

4.11. Detection of Ca^{2+} levels

SGC-7901 cells in 12-well plates were incubated with the fluorescent probe Fluo-3AM for 24 h after treatment with **Ir-1-Ir-3** to detect changes in intracellular Ca^{2+} levels. Fluo-3MA is easily cleaved by esterase to form Fluo-3, which will produce strong fluorescence when combined with Ca^{2+}. Fluorescent dyes in the wells that are not bound to the cells are washed three times with cold PBS. Finally, SGC-7901 cells were imaged by ImageXpress Micro XLS system (MD, US) and the fluorescence intensity of each well was calculated.

4.12. Release of cytochrome c

SGC-7901 cells were seeded in a 12-well plate and incubated overnight. Then cells were treated with different concentrations of the complexes for 24 h. Subsequently, the cells were fixed with ice-cold immunol staining fix solution for 30 min at room temperature. After blocking cells with immunol staining blocking buffer for 1 h, the cells were treated with the primary antibody against cytochrome c (1:50 dilution) overnight at 4 ^{o}C. Next, the plate was washed with immunol staining wash buffer three times and probed with Alexa Fluor 488-Labeled Goat Anti-Mouse IgG (1:500 dilution) in the dark for 1 h at room temperature. Finally, the cells were washed with immunol staining wash buffer three times and the cell nuclei were stained with DAPI. The images were obtained using ImageXpress Micro XLS system, and Multi Wavelength Cell Scoring module was used to analyze the data. The integrated intensity/cell which represents the fluorescence intensity of each cell was used to measure the release of cyto-c. The fluorescence intensity of each cell was calculated as the total fluorescence intensity divided by the number of cells.

4.13. Matrigel invasion assay

The BD Matrigel invasion chamber was used to investigate the ability of complexes to inhibit tumor cell invasion. After the matrix glue was placed in the invading chamber and solidified at 37 ^{o}C, the serum-free medium containing SGC-7901 cells and the corresponding concentration of **Ir-1**-**Ir-3** was placed in the

upper chamber. After incubation for 24 h, the cells were fixed with 4% paraformaldehyde and stained with 0.1% crystal violet. After removing the uninvaded cells in the upper chamber, the invading cells were photographed by optical microscope and the number was recorded. The experimental data were taken from the average of three independent experiments.

4.14. Cell cycle arrest studies

SGC-7901 cells with a density of 5×10^5 per well were plated in 6-well plates (Costar, Corning Corp, New York) and incubated until tightly attached. After the incubation, RPMI 1640 medium containing 10% FBS in the wells was removed and replaced with a new medium containing the corresponding concentration of **Ir-1-Ir-3**. After incubating for 24 h, the cell strain was obtained by trypsinization, and the cells were washed with cold PBS. After being fixed with 75% alcohol, 20 μL of RNAse (0.2 mg / mL) and 20 μL of propidium iodide (0.02 mg / mL) were suspended from the cell pellet and incubated for 30 min at room temperature.

4.15. Effects of the complexes on microtubule network

SGC-7901 cells in 12-well plates were treated with **Ir-1-Ir-3** for 24 h, and the cells were fixed with immunostaining fixative solution for 30 min. After removing the fixative solution, the cells were washed three times with cold PBS and incubated with the immunostaining blocking solution for 1 h at room temperature. After incubation and washing, SGC-7901 cells were incubated with anti-rabbit monoclonal

anti-α-tubulin antibody (1:100 dilution) overnight at 4 °C. After washing the cells three times with PBST, the cells were incubated with anti-rabbit FITC-conjugated IgG antibody (1:500 dilution) for 1 h, and then the nuclei were stained with Hoechst 33258. The cells was imaged and analyzed by ImageXpress Micro XLS system (MD, US).

4.16. Western blotting assay

When the SGC-7901 cells in the 6-well plate were attached and grown at a high density, the medium containing the corresponding concentration of **Ir-1-Ir-3** was replaced with the original medium and incubation was continued for 24 h. Rapidly obtain cell protein suspension by cell lysis buffer on ice bath, then perform low temperature high speed centrifugation for 15 min. After obtaining the supernatant, the concentration of the corresponding protein was determined by BCA (bicinchoninic acid) working solution. Add these processed proteins to the same amount of protein for sodium dodecyl sulfate-polyacrylamide gel electrophoresis using a micro syringe. The separation gel was transferred to a PVDF membrane, which was then blocked with TBST buffer containing 5% skim milk powder for 4 h. The PVDF membrane was washed four times with TBST buffer after overnight at 4 °C with the specific antibody selected for specificity. The labeled secondary antibody was incubated with the PDVF membrane bound to the primary antibody for 1 h at room temperature. The blots were visualized using Amersham ECL Plus western blotting detection reagents according to the manufacturer's instructions. To assess the presence of comparable

amounts of protein in each lane, the membranes were stripped finally to detect the β-actin.

4.17. Acute toxicity assay

Healthy Kunming (KM) mice (6-8 weeks old) weighing 18-22 g were housed in rooms in which the temperature was approximately 22-24 ^{o}C, with a relative humidity of 40-50%, and in a 12 h light-dark cycle was used. Sterile food and water were provided according to institutional guidelines. All animals were provided by the Laboratory Animal Center of Guangdong Pharmaceutical University. All animal procedures were approved by the Animal Ethical Committee of Guangdong Pharmaceutical University. Prior to each experiment, the mice were fasted overnight and allowed free access to water. Various doses of **Ir-3** ranging from 1 to 10 mg/kg dissolved in a 0.5% DMSO were administered intraperitoneally to different groups of healthy KM mice; each group contained 6 mice. After the compound had been administered, the mice were observed continuously for the first 2 h for any gross behavioral changes or death, intermittently for the next 24 h and thereafter for 10 days to determine the onset of any delayed effects. All animals were sacrificed at the 10 days after drug administration and checked macroscopically for possible damage to the heart, liver, and kidneys. Mice that died immediately following drug administration were also examined for any possible organ damage.

4.18. Antitumor activity assay

Mice with human tumor xenografts (HOS) were provided by the Laboratory Animal Center of Sun Yat-Sen University. Different doses of 0.75 and 1.50 mg/kg of **Ir-3** were injected intraperitoneally into mice of different group (each group contained 6 mice) once a day for seven consecutive days beginning 24 h after inoculation. This dose was the maximum tolerated dose based on our preliminary studies. Cisplatin (2 mg/kg) was used as a positive control. Control mice were injected with the vehicle. Compounds were administered by exact body weight, with the injection volume of 200 μL. The weights of the animals were recorded every day. All animals were sacrificed on the eighth days after tumor inoculation, and the tumors were excised and weighed. The inhibition rate was calculated as follow:

$$[(C - T)/C] \times 100\%$$

T is the average tumor weight of the treated group and C is the average tumor weight of the negative control group [81].

*4.19. **Ir-3** on histopathological study*

In order to evaluate the degree of damage of **Ir-3** to tumor tissues and other normal organs in nude mice, when the animals were sacrificed, the tumor, brain, heart, lung, liver and kidney of nude mice were taken and fixed with 4% paraformaldehyde for 24 hours. After fixation, each tissue was embedded in paraffin and cut into 5 μm sections. The sections were then stained with hematoxylin and eosin staining kits purchased from the Beyotime Biotechnology Institute.

4.20. Data analysis

All data was expressed as means ± SD. Statistical significance was evaluated by a t-test. Differences were considered to be significant when a *P value was less than 0.05.

Acknowledgements

This work was supported by the National Natural Science Foundation of China (21877018), the Natural Science Foundation of Guangdong Province (2016A030313728) and Special Funds of Key Disciplines Construction from Guangdong and Zhongshan cooperating.

References

[1] G. Rohini, J. Haribabu, K.N. Aneesrahman, N.S.P. Bhuvanesh, K. Ramaiah, R. Karvembu, A. Sreekanth, Polyhedron. 152 (2018) 147-154.

[2] A. Kumar, A. Kumar, R.K. Gupta, R.P. Paitandi, K.B. Singh, S.K. Trigun, M.S. Hundal, D.S. Pandey, J. Organometallic. Chem. 801 (2016) 68-79.

[3] A.Z. El-Sonbati, A.F. Shoair, A.A. El-Bindary, M.A. Diab, A.S. Mohamed, J. Mol. Liq. 209 (2015) 635-647.

[4] P.Y. Zhang, H.Y. Huang, Y. Chen, J.Q. Wang, L.N. Ji, H. Chao, Biomaterials. 53 (2015) 522-531.

[5] X. Chen, L.L. Sun, Y. Chen, X.L. Cheng, W.J Wu, L.N. J, H. Chao, Biomaterials. 58 (2015) 72-81.

[6] Y. Chen, L.P. Qiao, L.N. Ji, H. Chao, Biomaterials. 35 (2014) 2-13.

[7] Q. Du, LH. Guo, M. Tian, X. X. Ge, Y.L. Yang, X.Y. Jian, Z.S. Xu, Z.Z. Tian, Z. Liu, Organometallics. 17 (2018) 2880-2889

[8] T. Tanaka, M. Kasai, S. Kobayashi, Exp. Cell. Res. 370 (2018)454-460.

[9] G.Y. Li, Q. Lin, L.L. Sun, C.S. Feng, P.Y. Zhang, B.L. Yu, Y. Chen, H. Wang, L.N. Ji, H. Chao, Biomaterials. 53 (2015) 285-295.

[10] L. He, J.J. Cao, D.Y. Zhang, L. Hao, M.F. Zhang, C.P. Tan, L.N. Ji, Z.W. Mao,

Sensor Actuat B-Chem, 262 (2018) 313–325.

[11] J.S. Nam, M.G. Kang, J. Kang, S.Y. Park, S.J. Lee, H.T. Kim, J.K. Seo, O.H. Kwon, M.H. Lim, H.W. Rhee, T.H. Kwon, J. Am. Chem. Soc. 138(2016) 10968-10977.

[12] J.J. Cao, Y. Zheng, X.W. Wu, C.P. Tan, M.H. Chen, N. Wu, L.N. Ji, Z.W. Mao, J. Med. Chem. 62 (2019) 3311–3322.

[13] P.C.C. James, E.B. Hannah, J.I. Song, A.S. Nichola, P.E.B. Nicolas, I.B.P.J. Sadler, R.C. Isolda, J. Med. Chem. 61 (2018) 9246–9255.

[14] H.J. Zhong, W.H. Wang, T.S. Kang, H. Yan, Y.L. Yang, L.P. Xu, Y. Q. Wang, D.L. Ma, C.H. Leung, J. Med. Chem. 60 (2017) 497–503.

[15] Z.W. Mao, M.Q. Chen, X.S. Tan, J. Liu, W.X. Tang, Inorg. Chem. 34 (1995) 2889-2893.

[16] F.X. Wang, M.H. Chen, Y.N. Lin, H. Zhang, C.P. Tan, L.N. Ji, Z.W. Mao, ACS Appl. Mater. Inter. 9 (2017) 42471–42481.

[17] D.Y. Zhang, Y. Zheng, C.P. Tan, J.H. Sun, W. Zhang, L.N. Ji, Z.W. Mao, ACS Appl. Mater. Inter. 9 (2017) 6761-6771.

[18] W. Zhang, J. Shen, H. Su, G. Mu, J H. Sun, C.P. Tan, L.N. Ji, Z.W. Mao, ACS Appl. Mater. Inter. 8 (2016) 13332–13340.

[19] M. H. Chen, F. X. Wang, J. J. Cao, C. P. Tan, L. N. Ji, Z. W. Mao, ACS Appl. Mater. Inter. 9 (2017) 13304-13314.

[20] C. Gossens, I. Tavernelli, U. Rothlisberger, J. Am. Chem. Soc. 130 (2008) 10921-10928.

[21] F. Wang, J. Xu, A. Habtemariam, J. Bella, P. J. Sadler, J. Am. Chem. Soc. 127 (2014) 17734-17743.

[22] C. Haimei, J.A. Parkinson, P. Simon, R.A. Coxall, R.O. Gould, P.J. Sadler, J. Am. Chem. Soc. 124 (2002) 3064-3082.

[23] W. Bao, X.W. Liu, Y.L. Lv, G.H. Lu, F. Li, F. Zhang, B. Liu, D. Li, W. Wei, Y. Li, ACS. Nano. 13 (2019) 260–273.

[24] Q.Y. Yi, W.Y. Zhang, M. He, F. Du, X.Z. Wang, Y.J. Wang, Y.Y. Gu, L. Bai, Y.J. Liu, J. Biol. Inorg. Chem. 24 (2019) 151-169.

[25] B. Tang, D. Wan, Y.J. Wang, Q.Y. Yi, B.H. Guo, Y.J. Liu, Eur. J. Med. Chem. 145 (2018) 302-314.

[26] Q.Y. Yi, D. Wan, B. Tang, Y.Y. Wang, W.Y. Zhang, F. Du, M. He, Y.J. Liu, 145 (2018) 338-349.

[27] Y.Y. Wang, Q.Y. Yi, W.Y. Zhang, F. Du, M. He, Y.J. Liu, Polyhedron 156 (2018) 320-331.

[28] C. Zhang, S.H. Lai, H.H. Yang, D.G. Xing, C.C. Zeng, B. Tang, D. Wan, Y.J. Liu, RSC Adv. 7 (2017) 17752-17762.

[29] R.L. Guan, Y. Chen, L.L. Zeng, T.W. Rees, C.Z. Jin, J.J. Huang, Z.S. Chen, L.N. Ji, H. Chao, Chem. Sci. 9 (2018) 5183-5190.

[30] Y.M. Ou, L.L. Zeng, H.Y. Huang, C.Z. jin, Y. Chen, L.N. Ji, H. Chao, Dalton Trans. 46 (2017) 6734-6744.

[31] Y.L. Yang, L.H. Guo, X.X. Ge, S.P. Shi, Y.T. Gong, Z.S. Xu, X.F. Zheng, Z. Liu, J. Inorg. Biochem. 191 (2019) 1-7

[32] H.L. Hao, X.C. Liu, X.X. Ge, Y. Zhao, X. Tian, T. Ren, Y. Wang, C.F. Zhao, Z. Liu, J. Inorg. Biochem. 192 (2019) 52-61.

[33] C. Pérez-Arnaiz, M. I. Acuña, N. Busto, I. Echevarría, M. Martínez-Alonso, G. Espino, B. García, F. Domínguez, Eur. J. Med. Chem. 157 (2018) 279-293.

[34] C. Zhang, S.H. Lai, C.C. Zeng, B. Tang, D. Wan, J. Biol. Inorg. Chem. 21 (2016) 1047-1060.

[35] X.D. Song, Y. Qian, R. Ben, X. Lu, H.L. Zhu, H. Chao, J. Zhao, J. Med. Chem. 56 (2013) 6531-6535.

[36] V. Venkatesh, R. Berrocal-Martin, C.J. Wedge, I. Romero-Canelón, C. Sanchez-Cano, J.I. Song, J.P.C. Coverdale, P.Y. Zhang, G.J. Clarkson, A. Habtemariam, S.W. Magennis, R.J. Deeth, P.J. Sadler, Chem. Sci. 8 (2017) 8271-8278.

[37] T.S. Kang, Z.F. Mao, C.T. Ng, M. Wang, W.H. Wang, C.M. Wang, S.M.Y. Lee, Y.T. Wang, C.H. Leung, D.L. Ma, J. Med. Chem. 59 (2016) 4026-4031.

[38] F. Chen, J. Moat, D. McFeely, G. Clarkson, I.J. Hands-Portman, J.P. Furner-Pardoe, F. Harrison, C.G. Dowson, P.J. Sadler, J. Med. Chem. 61 (2018) 7330-7344.

[39] J.J. Cao, Y. Zheng, X.W. Wu, C.P. Tan, M.H. Chen, N.Wu, L.N. Ji, Z.W. Mao, J. Med. Chem. 62 (2019) 3311-3322.

[40] S. Lin, L.H. Lu, T.S. Kang, J.L. Mergny, C.H. Leung, D.L. Ma, Annal. Chem. 88 (2016) 10290-10295.

[41] H. Wang, L. Hu, W. Du, X. Tian, Q. Zhang, Z.J. Hu, L. Luo, H.P. Zhou, J.Y. Wu,

Y.P. Tian, ACS Biomater. Sci. Eng. 3 (2017) 836-842.

[42] D. Solairaj, P. Rameshthangam, G. Arunachalam, INT. J. Biol. Macromol. 105 (2017) 608-619

[43] S.D. Guggilapu, L. Guntuku, T.S. Reddy, A. Nagarsenkar, D.K. Sigalapalli, V.G.M. Naidu, S.K. Bhargava, B.N. Babu, Eur. J. Med. Chem. 138 (2017) 83-95.

[44] H.S. Jung, J. Han, J.H. Lee, J.H. Lee, J.M. Choi, H.S. Kweon, J.H. Han, J.H. Kim, K.M. Byun, J.H. Jung, C. Kang, J.S. Kim, J. Am. Chem. Soc. 137 (2015) 3017-3023.

[45] A. Mallick, P. More, M.M.K. Syed, S. Basu, Appl. Mater. Inter. 8 (2016) 13218-13231.

[46] J.H. Cui, X. Zhang, G. Huang, Q.J. Zhang, J.Y. Dong, G.G. Sun, Q.Q. Meng, S.S. Li, Mol. Pharmaceut. 16 (2019) 409-421.

[47] M.D. Altıntop, B. Sever, G.A. Çiftçi, T.Z. Gülhan, Z. A. Kaplancıklı, A. Özdemir, Eur. J. Med. Chem. 155 (2018) 905-924.

[48] W.Y. Zhang, Q.Y. Yi, Y.J. Wang, F. Du, M. He, B. Tang, D. Wan, Y.J. Liu, H.L. Huang, Eur. J. Med. Chem. 151 (2018) 568-584.

[49] M. Zhu, J.B. Wang, J.W. Xie, L.P. Chen, X.Y. Wei, X. Jiang, M. Bao, Y.Y. Qiu, Q. Chen, W.L. Li, C.X. Jiang, X.O. Zhou, L.P. Jiang, P.H. Qiu, J.Z. Wu, Eur. J. Med. Chem. 157 (2018) 1395-1405.

[50] D.S. Kalinowski, P.C. Sharpe, P.V. Bernhardt, D.R. Richardson, J. Med. Chem. 50 (2007) 6212-25.

[51] F. Dai, W.J. Yan, X. Fu, Y.L. Zheng, Y.T. Du, X.Z. Bao, Y.F. Kang, X.L. Jin, B.

Zhou, Eur. J. Med. Chem. 159 (2018) 317-323.

[52] J.J. Chen, Z.D. Luo, Z.N. Zhao, L.N. Xie, W.J. Zheng, T.F. Chen. Data In Brief. 8 (2016) 670-686.

[53] K.J. Wu, H.J. Zhong, G.J. Yang, C. Wu, J.M. Huang, G.D. Li, D.L. Ma, C.H. Leung, Chem-An Asian J. 13 (2018) 275-279.

[54] C.C. Hsu, J.C. Lien, C.W. Chang, C.H. Chang, S.C. Kuo, T.F. Huang, Biochemical Pharmacology, 85 (2013) 385-395.

[55] K.J. Wu, H.J. Zhong, G.D. Li, C.F. Liu, H.M.D. Wang, D.L. Ma, C.H. Leung, Eur. J. Med. Chem. 143 (2018) 1021-1027.

[56] Q.C. Huang, L. Zhan, H.Y. Cao, J.B. Li, Y.H. Lyu, X. Guo, J. Zhang, L.L. Ji, T.T. Ren, J.Z. An, B.R. Liu, Y.Z. Nie, J.L. Xing, Autophagy, 2016, 12 (2016) 999-1014.

[57] R.P. Nishanth, R.G. Jyotsna, J.J. Schlager, S.M. Hussain, P. Reddanna, Nanotoxicology, 5 (2011) 502-516.

[58] J.H. Gao, G.L. Liang, B. Zhang, Y. Kuang, X.X. Zhang, B. Xu, J. Am. Chem. Soc. 16 (2019) 409-421.

[59] P. Naveen, F. Dallemer, R.J. Butcher, R. Prabhakaran, Inorg. Chim. Acta. 471 (2018) 724-734.

[60] S. Sampath, V. Veeramani, G.S. Krishnakumar, U. Sivalingam, S.L. Madurai, R. Chellan, Biomed. Pharmacotcher 93 (2017) 296-307.

[61] C. Bartel, A.K. Bytzek, Y.Y. Scaffididomianello, G. Grabmann, M.A. Jakupec, C.G. Hartinger, M. Galanski, B.K. Keppler, J. Biol. Inorg. Chem. 17 (2012)

465-474.

[62] P. Jost, H. Svobodova, R. Stetina, Chem-Biol. Interact. 237 (2015) 31-37.

[63] M. Novak, B. Žegura, B. Modica, E. Heathd, M. Filipič, Sci. Total. Environ. 601-602 (2017) 293-300.

[64] X.D. Xu, Y. Zhao, M. Zhang, R.Z. He, X.H. Shi, X.J. Guo, C.J. Shi, F. Peng, M. Wang, M. Shen, X. Wang, X. Li, R.Y. Qin, Int. J. Mol. Sci. 18 (2017) 370.

[65] V. Pooladanda, S. Bandi, S.R. Mondi, K.M. Gottumukkala, C. Godugu, Toxicol. In. Vitor. 51 (2018) 114-128.

[66] Y.L. Li, P.H. Luo, J.C. Wang, J.B. Dai, X.C. Yang, H.H. Wu, B. Yang, Q.J. He, Toxicol. Appl. Pharm. 274 (2014) 319-327.

[67] J. Das, S. Das, A. Paul, A. Samadder, A.R. Khuda-Bukhsh, J. Acupunct. Meridian. Stud. 7 (2014) 140-150.

[68] Y. Yu, Q. Xie, W. Liu, Y. Guo, N. Xu, L. Xu, S.B. Liu, S.Y. Li, Y. Xu, L.K. Sun, Biomed. Pharmacother. 86 (2017) 8-15.

[69] L.Y. Jin, L. Changhee, Virus. Res. 253 (2018) 112-123.

[70] H.Y. Wu, C.H. Huang, Y.H. Lin, C.C. Wang, T.R. Jan, FREE. Radical. Bio. Med. 124 (2018) 311-318.

[71] S.P. Yang, Y.G. Zhang, Y. Luo, B.C. Xu, Y.Q. Yao, Y.L. Deng, F.F. Yang, T.H. Ye, G. Wang, Z.Q. Cheng, Y. Zheng, Y.M. Xie, Biomed. Pharmacother. 103 (2018)101-110.

[72] Q. Zhou, C.Q. You, C. Zheng, Y.W. Gu, H.C. Gu, R. Zhang, H.S. Wu, B.W. Sun, Life. Sci 206 (2018) 1-9.

[73] X. Cai, L. Guo, F. Pei, X. Chang, R. Zhang, Arch. Biochem. Biophys. 644 (2018) 93-99.

[74] X. Tian, J. Zhang, F. Zhang, M. Zhao, X. Mei, Colloid. Surface. B. 165 (2018).278-285.

[75] S. Cheriyamundath, T. Mahaddalkar, S.N. Save, S. Choudhary, R.V. Hosur, M. Lopus, Biomed. Pharmacother. 98 (2018) 76-81.

[76] M. Koronkiewicz, Z. Chilmonczyk, Z. Kazimerczuk, A. Orzeszko, Eur. J. Pharmacol. 820 (2018) 146-155.

[77] J. Zhan, F. Feng, W. Qu, C.l. Wang, W. Kitdamrongtham, A. Manosroi, J. Manosroi, H. Tokuda, M. Abe, T. Akihisa, J. Ethnopharmacol. 214 (2018) 37-46.

[78] S.H. Lai, G.B. Jiang, J.H. Yao, W. Li, B.J. Han, C. Zhang, C.C. Zeng, Y.J. Liu, J. Inorg. Biochem.152 (2015) 1-9.

[79] S. Sprouse, K.A. King, P.J. Spellane, R.J. Watts, J. Am. Chem. Soc. 106 (1984) 6647-6653.

[80] G. Ding, F. Liu, T. Yang, Y. Jiang, H. Fu, Y. Zhao, Bioorg. Med. Chem. 14 (2006) 3766-3774.

[81] R.H. Cao, Q. Chen, X.R. Hou, H.S. Chen, H.J. Guan, Y. Ma, W.L. Peng, A.L. Xu, Bioorg. Med. Chem. 12 (2004) 4613-4623.

Captions for Schemes and Figures

Table 1 IC_{50} (μM) values of complexes toward selected cell lines.

Scheme 1 Synthetic route of complexes **Ir-1**, **Ir-2** and **Ir-3**

Fig. 1 (A) Location assays of the complexes in the mitochondria. (B) The change in the mitochondrial membrane potential after SGC-7901 cells (a) were treated with CCCP (b, positive control), 2.0 μM **Ir-1** (c) and 1.0 μM **Ir-2** (d) and **Ir-3** (e) for 24 h. (C) The ratio of red/green fluorescence intensity was determined after SGC-7901 cells (a), SGC-7901 + NAC (b) were incubated with complexes **Ir-1** (c, 1.0 μM), **Ir-1** (d, 2.0 μM), **Ir-1** (2.0 μM) + NAC (e); **Ir-2** (f, 1.0 μM), **Ir-2** (g, 2.0 μM), **Ir-2** (2.0 μM) + NAC (h) and **Ir-3** (i, 1.0 μM), **Ir-2** (j, 2.0 μM), **Ir-2** (2.0 μM) + NAC (k) for 24 h.

Fig. 2 Intracellular ROS was detected in SGC-7901 cells (a) exposure to ROSUP (b, positive control), 2.0 μM of **Ir-1** (c), **Ir-2** (d) and 1.0 μM of **Ir-3** (e) for 24 h. (B) the DCF fluorescence intensity was determined after SGC-7901 cells were exposed to ROSUP and 2.0 μM of **Ir-1**, **Ir-2** and 1.0 μM of **Ir-3** in the absence or presence of NAC for 24 h. (C) $O_2^{\bullet-}$ level was detected in SGC-7901 cells (a) exposure to 2.0 μM of **Ir-1** (b), **Ir-2** (c) and 1.0 μM of **Ir-3** (d) for 24 h. (D) the DHE fluorescence intensity was determined after

SGC-7901 cells were exposed to 2.0 μM of **Ir-1**, **Ir-2** and 1.0 μM of **Ir-3** in the absence or presence of NAC for 24 h. (E) NO level was detected in SGC-7901 cells (a) exposure to 2.0 μM of **Ir-1** (b), **Ir-2** (c) and 1.0 μM of **Ir-3** (d) for 24 h. (F) the DAF-FMDA fluorescence intensity was determined after SGC-7901 cells were exposed to 2.0 μM of **Ir-1**, **Ir-2** and 1.0 μM of **Ir-3** in the absence or presence of NAC for 24 h. (G) The expression of p38MAPK induced by 2.0 μM of **Ir-1**, **Ir-2** and 1.0 μM of **Ir-3** for 24 h. $*P < 0.05$ represents significant differences compared with control.

Fig. 3 (A) Apoptosis assays of SGC-7901 cells (a) exposed to 2.0 μM of Ir-**1** (b), Ir-2 (c) and 1.0 μM of **Ir-3** (d) for 24 h and the cell nuclei were stained with AO/EB. (B) The apoptotic percentage of SGC-7901 cells (a) were treated with 2.0 μM of **Ir-1** (b), **Ir-2** (c) and 1.0 μM **Ir-3** (d) for 48 h.

Fig. 4 Comet assays of SGC-7901 (a) exposure to 2.0 μM of **Ir-1** (b), **Ir-2** (c) and 1.0 μM of **Ir-3** (d) for 24 h.

Fig. 5 (A) Autophagy was assayed after SGC-7901 cell (a) was treated with 2.0 μM of **Ir-1** (b), **Ir-2** (c) and 1.0 μM of **Ir-3** (d) for 24 h. (B) The expression of p62, Beclin-1 and LC3 while SGC-7901 cells were exposed to 2.0 μM of **Ir-1** (b), **Ir-2** (c) and 1.0 μM of **Ir-3** (d) for 24 h.

Fig. 6 Relationship between cell viability and ROS or autophagy after SGC-7901 cells were incubated with 2.0 μM of **Ir-1** (b), **Ir-2** (c) and 1.0 μM of **Ir-3** (d) in the absence or presence of NAC or 3-MA for 24 h.

Fig. 7 (A) Intracellular Ca^{2+} levels were assayed after SGC-7901 cells (a) were

exposed to Ca^{2+} free medium (b), 2.0 μM of **Ir-1** (c), **Ir-2** (d) and 1.0 μM of **Ir-3** (e) for 24 h. (B) Fluo-3 fluorescent intensity compared with the control was determined after SGC-7901 cells were treated with Ca^{2+} free medium, 2.0 μM of **Ir-1**, **Ir-2** and 1.0 μM of **Ir-3** for 24 h.

Fig. 8 (A) The release of cytochrome c was assayed after SGC-7901 cells (a) were exposed to 2.0 μM of **Ir-1**, **Ir-2** and 1.0 μM of **Ir-3** for 24 h. (B) The integrated fluorescent intensity/cell compared with control was determined after the treatment of SGC-7901 cells with 2.0 μM of **Ir-1**, **Ir-2** and 1.0 μM of **Ir-3** for 24 h. $*P < 0.05$ represents significant differences compared with control.

Fig. 9 (A) Cell invasion of SGC-7901 cells (a) that have migrated through the Matrigel induced by 2.0 μM of **Ir-1** (b), **Ir-2** (c) and 1.0 μM of **Ir-3** (d) for 24 h. (B) Inhibiting percentage of cell invasion induced by different concentration of complexes **Ir-1**, **Ir-2** and **Ir-3** for 24 h. $*P < 0.05$ represents significant differences compared with control.

Fig. 10 Cell cycle distribution of SGC-7901 cells (a) exposure to 2.0 μM of **Ir-1** (b), **Ir-2** (c) and 1.0 μM of **Ir-3** (d) for 24 h.

Fig. 11 Assays of microtubules network of SGC-7901 cells (a) induced by 2.0 μM of **Ir-1** (b), **Ir-2** (c) and 1.0 μM of **Ir-3** (d) for 24 h.

Fig. 12 (A) Western blot analysis of p53, Cleaved PARP, caspase 3, Bcl-2 family protein in SGC-7901 cells treated with 2.0 μM of **Ir-1**, **Ir-2** and 1.0 μM of **Ir-3** for 24 h. β-actin was used as internal control.

Fig. 13 The in vivo antitumor activity of complex **Ir-3** against SGC-7901 xenograft model (A) Relative volume of tumor. (B) Photographs of tumor from treatment groups and vehicle group. (C) Tumor weight (Mean ± SD) g after the tumor was treated with the complex **Ir-3** for 7 days. (D) Inhibiting percentage of tumor growth induced by cisplatin and different concentrations of complex **Ir-3**. $*P < 0.05$ represents significant differences compared with control.

Fig. 14 Effect of cisplatin and complex **Ir-3** on the tissue: Lung, heart, liver, brain and tumor compared to the control group.

Fig. 15 The apoptotic mechanism induced by the complexes **Ir-1**, **Ir-2** and **Ir-3**.

Table 1 IC_{50} values of the complexes toward the selected cancer cell lines

Complex	SGC-7901	A549	HeLa	Eca-109	HepG2	BEL-7402	NIH 3T3
NDPPZ	82.1 ± 4.3	> 100	82.8 ± 3.5	81.6 ± 4.4	> 200	> 200	> 200
Ir-1	1.8 ± 0.4	3.6 ± 0.2	3.6 ± 0.6	4.9 ± 0.5	5.2 ± 0.5	5.7 ± 0.7	6.4 ± 1.0
Ir-2	1.6 ± 0.3	4.2 ± 0.8	4.1 ± 1.1	5.7 ± 0.5	6.3 ± 1.4	5.5 ± 0.8	6.1 ± 0.9
Ir-3	0.8 ± 0.1	3.4 ± 0.2	4.1 ± 0.2	4.5 ± 1.2	5.7 ± 1.3	4.4 ± 1.2	8.3 ± 1.7
Cisplatin	3.6 ± 0.5	7.5 ± 1.3	7.0 ± 1.0	11.2 ± 0.6	12.5 ± 1.5	10.8 ± 1.6	ND

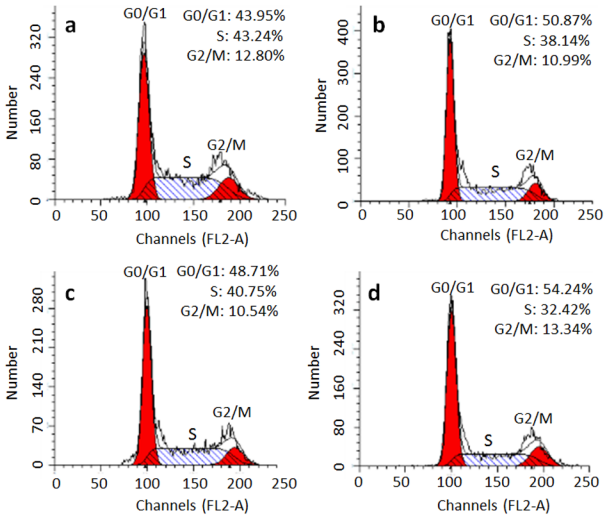

Fig.10

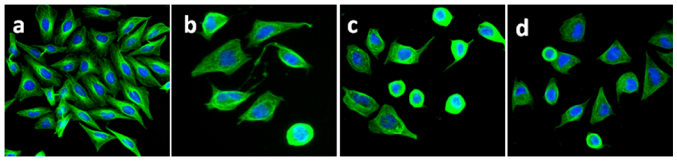

Fig. 11

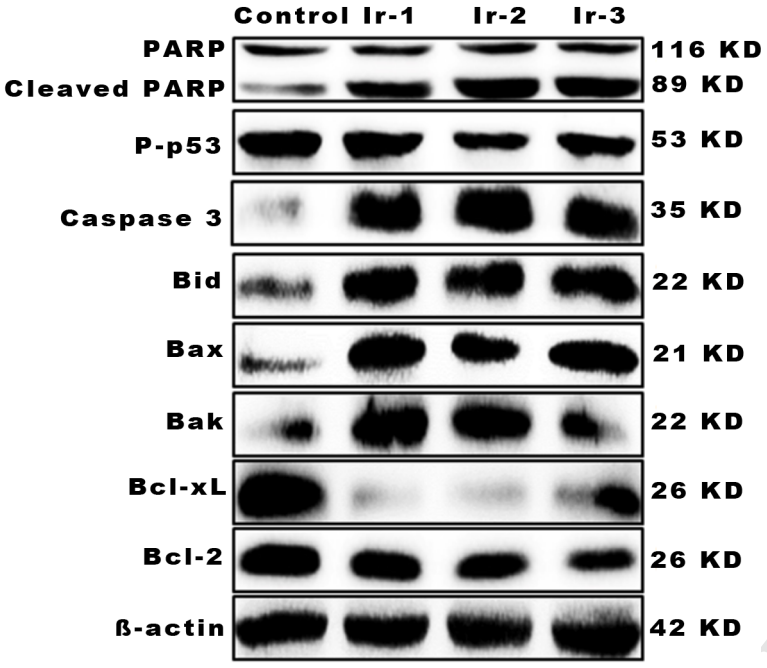

Fig. 12

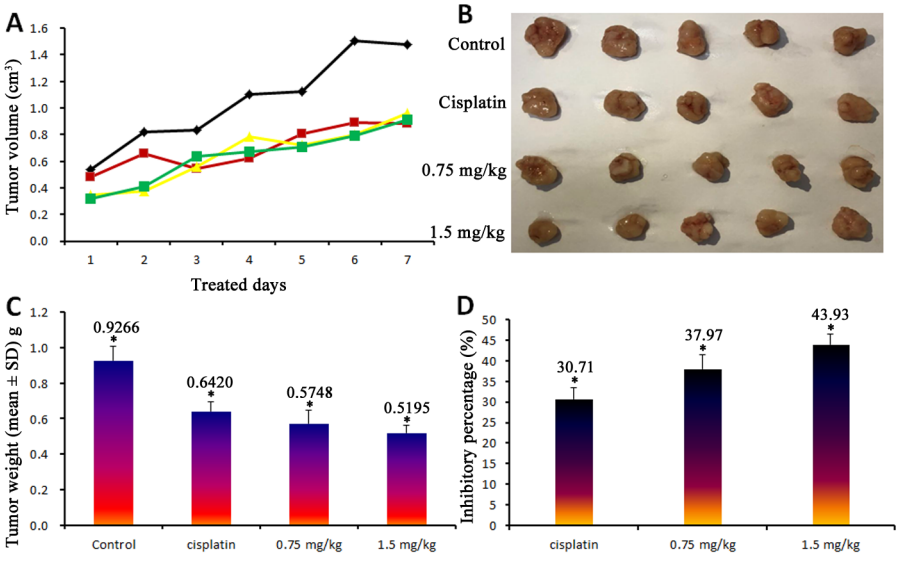

Fig. 13

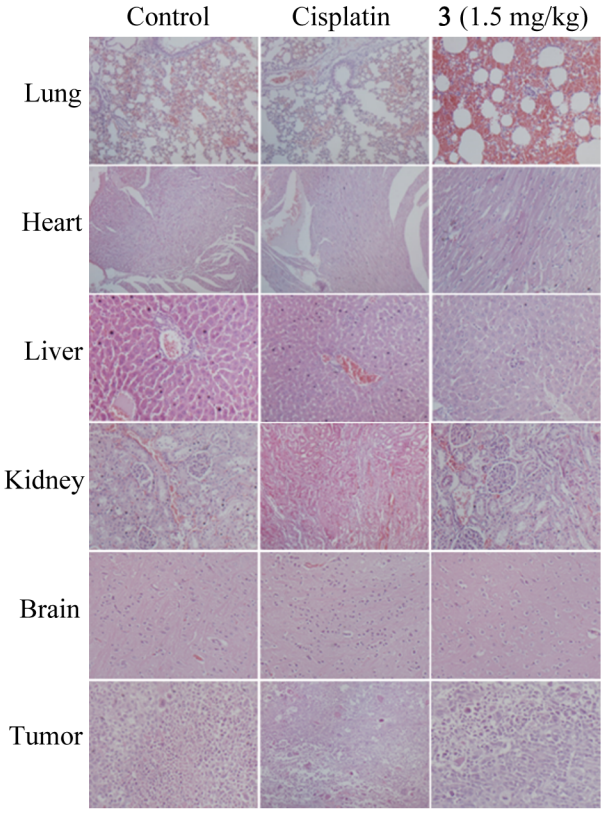

Fig. 14

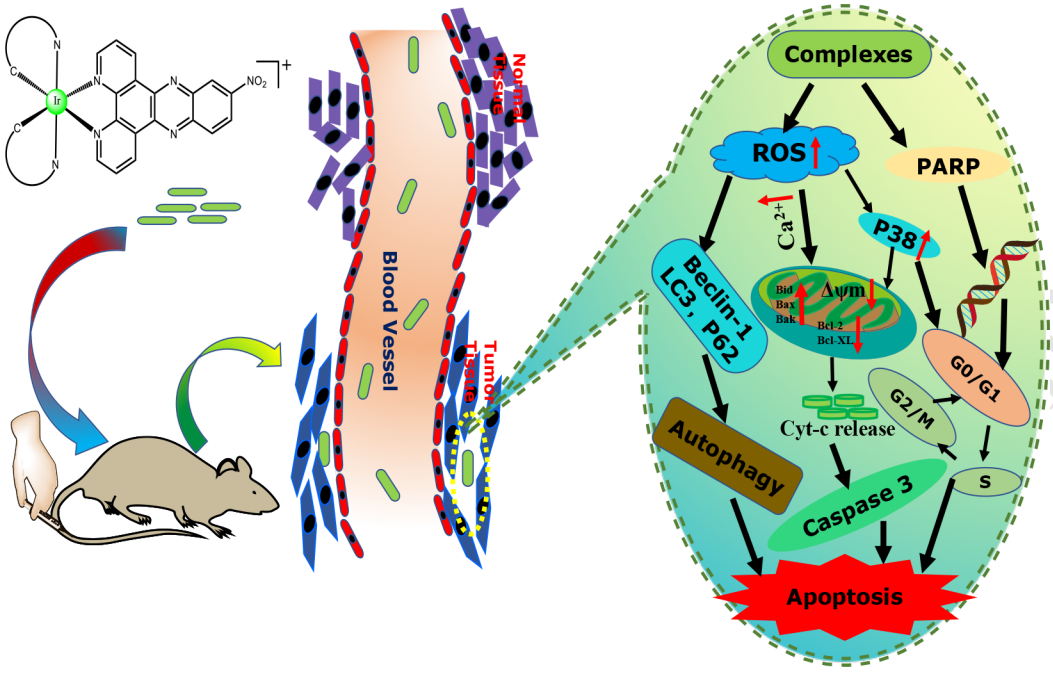

Fig. 15

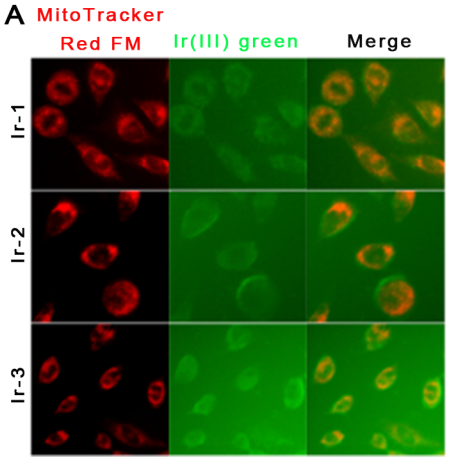

Fig. 1A

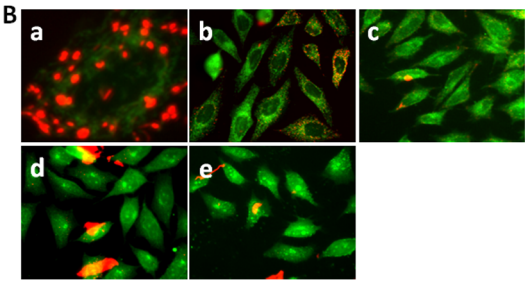

Fig. 1B

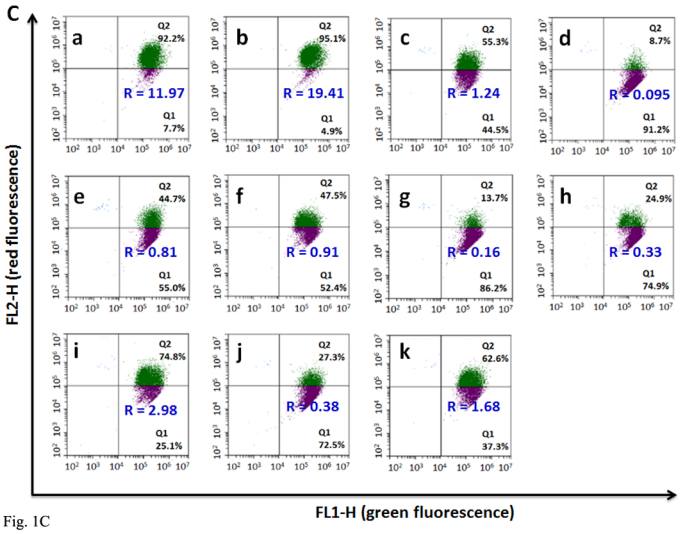

Fig. 1C

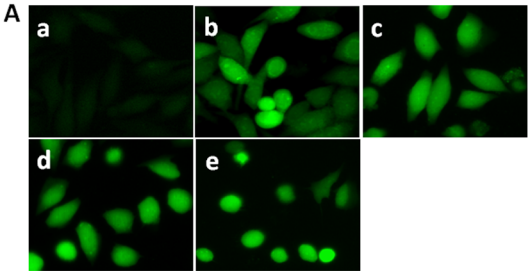

Fig. 2A

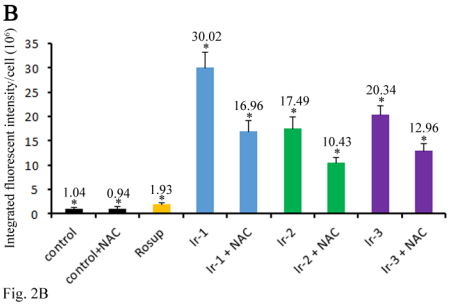

Fig. 2B

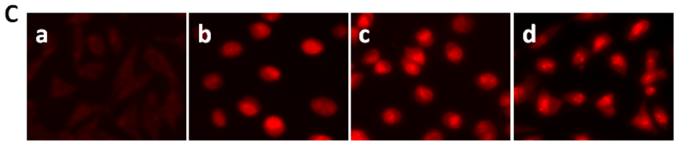

Fig. 2C

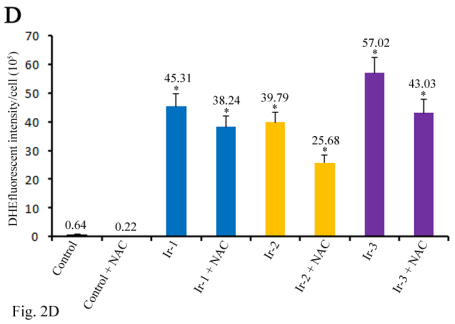

Fig. 2D

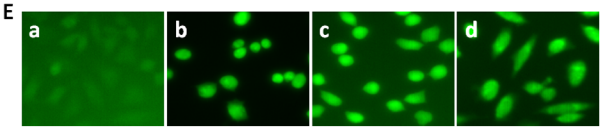

Fig. 2E

F

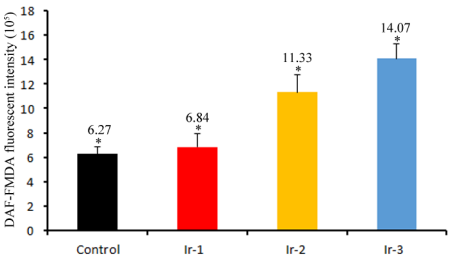

Fig. 2F

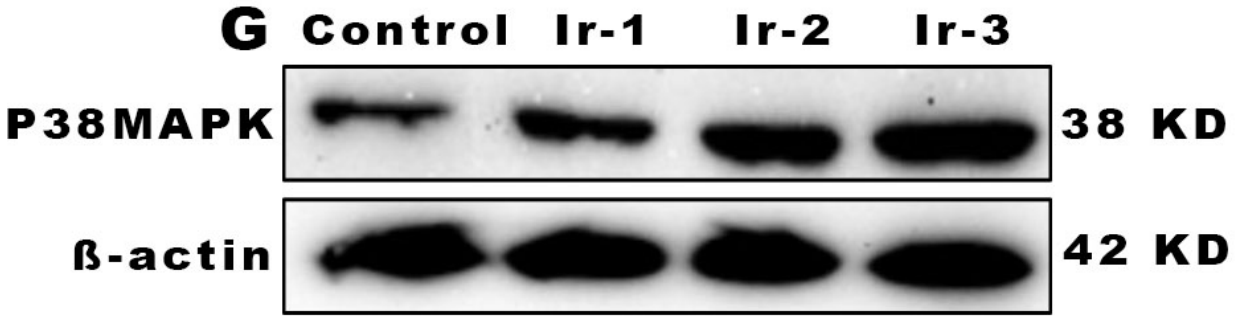

Fig. 2G

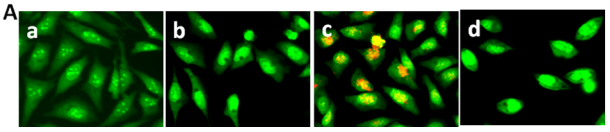

Fig. 3A

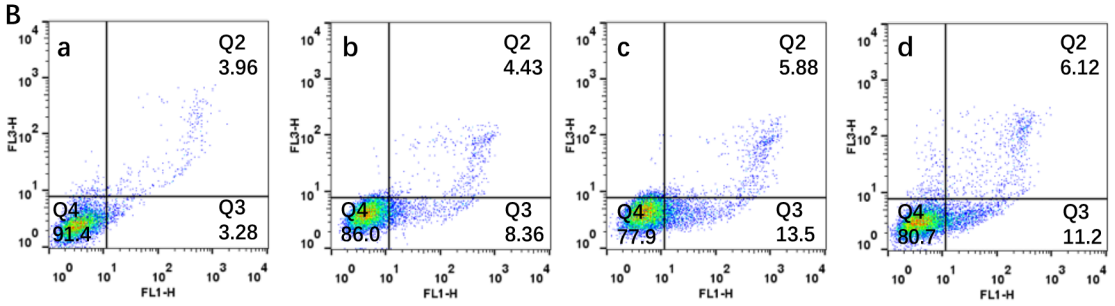

Fig. 3B

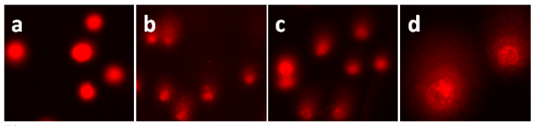

Fig. 4

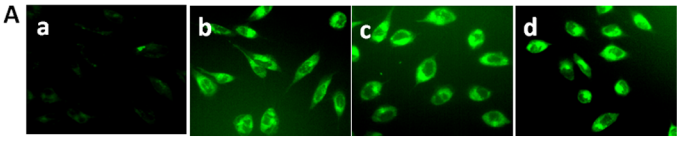

Fig. 5A

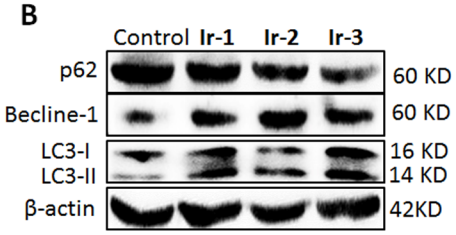

Fig. 5B

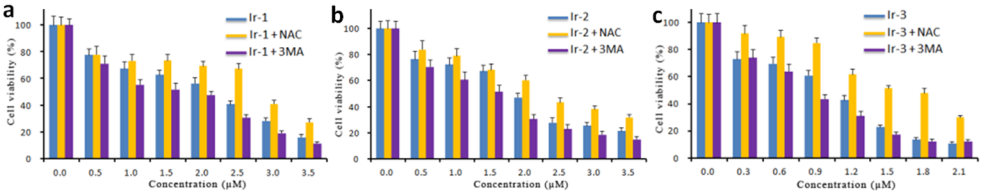

Fig. 6

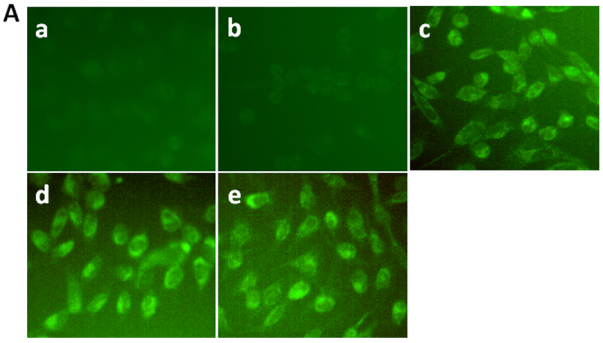

Fig. 7A

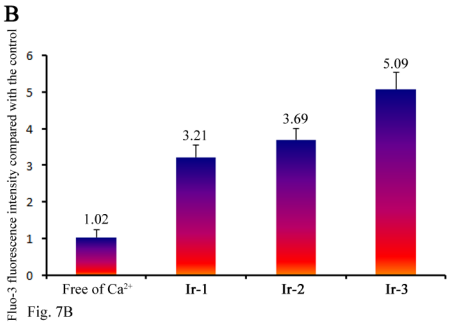

Fig. 7B

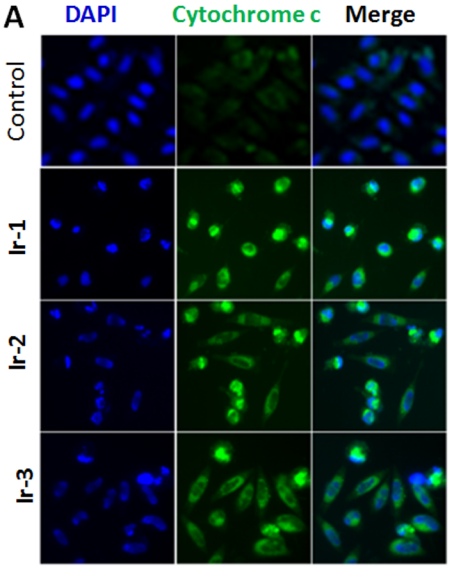

Fig. 8A

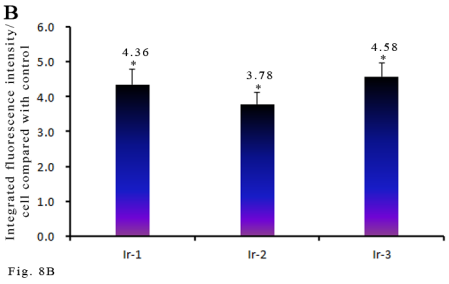

Fig. 8B

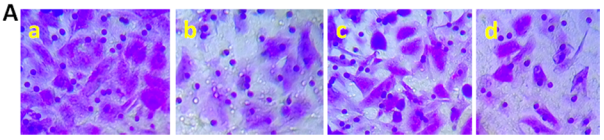

Fig. 9A

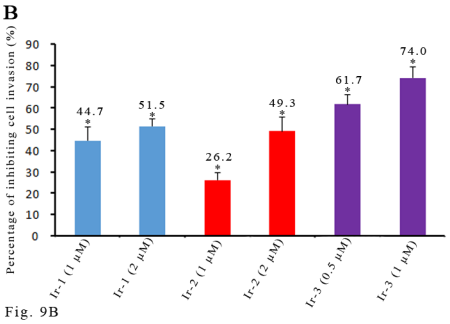

Fig. 9B

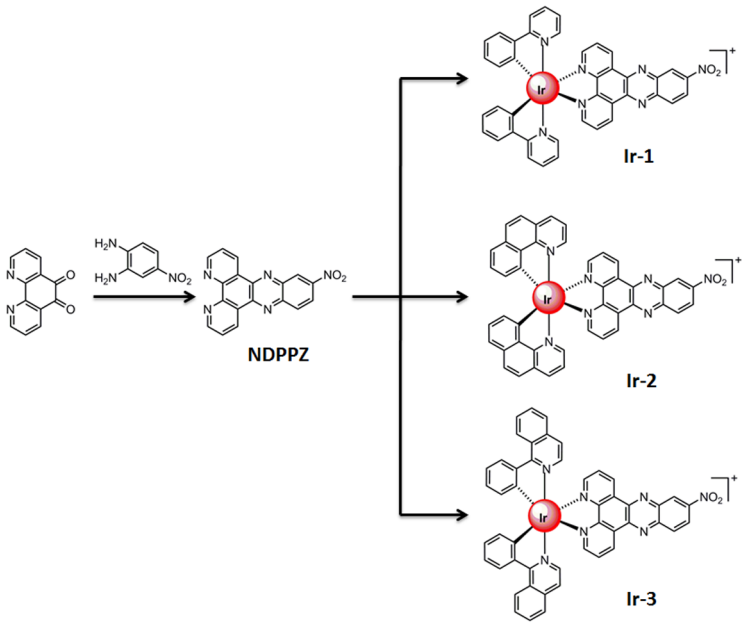

Scheme 1

Highlights

- The iridium(III) complexes were synthesized and characterized.
- The cytotoxicity in vitro was studied by MTT method
- The apoptosis, cell cycle arrest and intracellular ROS levels were assayed
- The effect of the complex on the tumor growth was evaluated